UNIVERSIDADE ESTADUAL PAULISTA
"JÚLIO DE MESQUITA FILHO"
Campus de Ilha Solteira

RICARDO FONSECA BUZO

NOVO MÉTODO PARA LOCALIZAÇÃO DE FALTAS EM REDES DE DISTRIBUIÇÃO DE ENERGIA ELÉTRICA BASEADO EM MEDIDAS ESPARSAS DE TENSÃO

Ilha Solteira
2020

UNIVERSIDADE ESTADUAL PAULISTA
"JÚLIO DE MESQUITA FILHO"
Campus de Ilha Solteira

RICARDO FONSECA BUZO

A NEW METHOD FOR FAULT LOCATION IN ELECTRICAL DISTRIBUTION SYSTEMS BASED ON SPARSE VOLTAGE MEASUREMENTS

Ph.D. thesis presented to the Faculty of Engineering, Campus of Ilha Solteira – UNESP, as part of the requirements for obtaining the title of Ph.D. in Electrical Engineering. Field of knowledge: Automation.

Prof. Dr. Fábio Bertequini Leão
Orientador

Ilha Solteira
2020

FICHA CATALOGRÁFICA

Desenvolvido pelo Serviço Técnico de Biblioteca e Documentação

B989n

Buzo, Ricardo Fonseca.

Novo método para localização de faltas em redes de distribuição de energia elétrica baseado em medidas esparsas de tensão / Ricardo Fonseca Buzo. -- Ilha Solteira: [s.n.], 2020

55 f. : il.

Tese (doutorado) - Universidade Estadual Paulista. Faculdade de Engenharia de Ilha Solteira. Área de conhecimento: Automação, 2020

Orientador: Fábio Bertequini Leão

Inclui bibliografia

1. Redes de distribuição. 2. Medidas esparsas. 3. Subsistemas. 4. Geração Distribuída. 5. Localização de faltas.

Raiane da Silva Santos

Raiane da Silva Santos

Supervisora Técnica de Seção

Seção Técnica de Referência, Atendimento ao usuário e Documentação

Diretoria Técnica de Biblioteca e Documentação

CRB/8 - 9999

unesp
UNIVERSIDADE ESTADUAL PAULISTA
Câmpus de Ilha Solteira

CERTIFICADO DE APROVAÇÃO

TÍTULO DA TESE: Novo Método de Localização de Faltas em Redes de Distribuição de Energia Elétrica baseado em Medidas Esparsas de Tensão

AUTOR: RICARDO FONSECA BUZO
ORIENTADOR: FABIO BERTEQUINI LEÃO

Aprovado como parte das exigências para obtenção do Título de Doutor em ENGENHARIA ELÉTRICA, área: Automação pela Comissão Examinadora:

Fábio Bertequini Leão.
Prof. Dr. FABIO BERTEQUINI LEÃO
Departamento de Engenharia Elétrica / Faculdade de Engenharia de Ilha Solteira - UNESP

Prof. Dr. CARLOS ROBERTO MINUSSI
Departamento de Engenharia Elétrica / Faculdade de Engenharia de Ilha Solteira - UNESP

Prof. Dr. JOSE ROBERTO SANCHES MANTOVANI
Departamento de Engenharia Elétrica / Faculdade de Engenharia de Ilha Solteira - UNESP

Prof. Dr. MÁRIO OLESKOVICZ
Departamento de Engenharia Elétrica e de Computação / Escola de Engenharia de São Carlos - USP

Rodrigo Pereira
Prof. Dr. RODRIGO APARECIDO FERNANDES PEREIRA
Departamento de Engenharia Elétrica / Universidade Tecnologica Federal do Paraná - UTFPR

Ilha Solteira, 14 de fevereiro de 2020

“*In all your ways acknowledge him, and he will make straight your paths.*”

Proverbs 3:6

ACKNOWLEDGMENT

To God,
for your, grace, mercy and support that gave me enough health and determination to do this job.

My wife,
for always providing, in all senses, a favorable scenario for carrying out the work.

To my parents and in-laws,
for all moral and financial support.

To my advisor,
for all the guidance, patience and immeasurable teachings.

To professors Mantovani and Jônatas,
for all contributions during the doctorate.

To professors Mário Oleskovicz, Rodrigo Pereira and Carlos Roberto Minussi,
for all important contributions made to the work.

To Henrique and Rárison,
for the friendships and partnerships made during the doctorate.

To CNPq,
for the scholarship and financial assistance that made possible the full dedication to the postgraduate program.

RESUMO

Neste trabalho, um novo algoritmo de localização de faltas é proposto com base em medições de tensão esparsas sincronizadas e não sincronizadas. Para tornar o método proposto mais acessível, tecnicamente, neste trabalho apresenta-se um novo procedimento de manipulação da matriz de impedância que cria diferentes subsistemas. Tal procedimento permite que o processo de localização de faltas seja realizado por meio da resolução de sistemas determinados de equações, o que reduz a complexidade durante a localização das faltas. Para reduzir os efeitos da geração distribuída (GD), um novo conceito é apresentado para o cálculo da corrente de falta, onde dispositivos de medição não são requeridos em barras com GD. O local da falta é identificado via análise da variação de tensão na barra terminal de cada subsistema. O desempenho do método proposto é avaliado em três sistemas de distribuição diferentes com/sem GD. O software DIgSILENT® é utilizado para modelar as redes de distribuição. Os resultados da simulação mostram a robustez do método em vários cenários pré-falta e pós-falta e erros de medição.

Palavras-chave: Redes de distribuição. Medidas esparsas. Subsistemas. Geração distribuída. Localização de faltas.

ABSTRACT

In this work, a new fault location algorithm is proposed based on sparse synchronized and non-synchronized voltage measurements. To make the proposed method more technically accessible, this work presents a new impedance matrix manipulation procedure that creates different subsystems. Such a procedure allows the fault location process to be carried out by solving determined systems of equations, which reduces the complexity during the fault location. To reduce the effects of distributed generation (DG), a new concept is presented for the fault current calculation, where measuring devices are not required at buses with DG. The fault is located by analyzing the voltage sag at the terminal-bus of each subsystem. The performance of the proposed method is evaluated in three different distribution systems with/without DG. DIgSILENT® software is used to model distribution networks. The simulation results show the robustness of the proposed method under several pre- and during-fault scenarios and measurement errors.

Keywords: Distribution networks. Sparse measurements. Subsystems. Distributed generation. Fault location.

LIST OF FIGURES

Figure 1 – 8-bus distribution system under fault condition at bus-6 18
Figure 2 – 8-bus distribution system under fault condition at section 5-6 20
Figure 3 – Section 2-3 under three different fault scenarios 21
Figure 4 – 8-bus distribution system with a reduced number of μPMUs 23
Figure 5 – 8-bus distribution system without buses 3, 5, 6, and 7 24
Figure 6 – 8-bus distribution system with DG at bus-7 25
Figure 7 – (a) 7-bus distribution system; (b) Proposed subsystems 28
Figure 8 – Subsystem 3 only with bus-1 and bus-7, both equipped with μPMU 29
Figure 9 – Fault current calculation procedure under DG presence 30
Figure 10 – Section h-k under two different fault locations 34
Figure 11 – Subsystem 1 with fictitious buses 35
Figure 12 – Subsystems 1, 2, and 3 with fictitious buses at different sections 36
Figure 13 – Subsystems 1, 2, and 3 with fictitious buses in the same section 1-2 37
Figure 14 – Flowchart of the proposed method for fault location 38
Figure 15 – The 8-bus distribution system under different scenarios 39
Figure 16 – Faulted subsystem of scenario 3 40
Figure 17 – Diagram of the 33-bus, 12.66 kV distribution system 42
Figure 18 – (a) Proposed subsystems used to inject the calculated fault current; (b) Proposed subsystems used to calculate the fault current 43
Figure 19 – Diagram of the 33-bus, 12.66 kV distribution system with DGs 49
Figure 20 – Graph of Error (%) versus SDG (kVA) for LG fault at 50% of section 12-13 when DG is placed at bus-25 52
Figure 21 – Graph of Error (%) versus S_{DG} (kVA) for LG fault at 50% of section 12-13 when DG is placed at bus-23 52
Figure 22 – Diagram of the 69-bus, 12.66 kV distribution system 53
Figure 23 – 134-bus distribution system 55

LIST OF TABLES

Table 1 – Primitive impedance matrix (ohm/km) applied to all sections of the 8-bus system. 22
Table 2 – Candidate bus of each subsystem for different fault distances 34
Table 3 – Fault location results when a fault occurs at bus-6 of the 8-bus system 40
Table 4 – Voltage profile at buses 1 and 18 of the 33-bus system 43
Table 5 – Fault current value when an LG fault occurs at section 5-6 of the 33-bus system .. 44
Table 6 – Fault current value calculated by each subsystem 44
Table 7 – Fault simulation results under different fault resistances 45
Table 8 – Method sensitivity to the fault resistances 46
Table 9 – Simulation results under unbalanced system condition 46
Table 10 – Simulation results for different loading scenarios 47
Table 11 – Errors attributed arbitrarily to the impedance of some sections 47
Table 12 – Simulation results under line parameter errors 48
Table 13 – Errors attributed arbitrarily to the measuring devices 48
Table 14 – Simulation results under voltage measurement errors condition 48
Table 15 – Simulation results under voltage measurement errors condition 49
Table 16 – Data of the distributed generators installed in the 33-bus system (configuration 1) 50
Table 17 – Simulation results under DG presence allocated according to Table 16 50
Table 18 – Simulation results under DG presence allocated according to Table 19 50
Table 19 – Data of the distributed generators installed in the 33-bus system (configuration 2) 51
Table 20 – Cases in which adjacent sections were indicated incorrectly in the 33-bus system 51
Table 21 – Method sensitivity to the loads model 53
Table 22 – Data of the distributed generators installed in the 69-bus system 54
Table 23 – Simulation results for the 69-bus system 54
Table 24 – Cases in which adjacent sections were indicated incorrectly in the 69-bus system 55
Table 25 – Simulation results for the 134-bus system 56
Table 26 – Distributed generations installed at the 134-bus system 57
Table 27 – Detailed simulation results for the 134-bus system without DG 57
Table 28 – Detailed simulation results for the 134-bus system with DG 59

SUMMARY

1 INTRODUCTION 10

2 LITERATURE REVIEW 12

3 CLASSICAL FAULT CURRENT CALCULATION 18

3.1 FAULT CURRENT CALCULATION CONSIDERING MEASURING DEVICES AT ALL BUSES 18
3.2 FAULT CURRENT CALCULATION REDUCING THE NUMBER OF MEASURING DEVICES 23
3.3 FAULT CURRENT CALCULATION UNDER DG PRESENCE 25

4 PROPOSED METHOD FOR FAULT LOCATION 28

4.1 FAULT CURRENT CALCULATION 29
4.2 LOCATING THE BUS CLOSEST TO THE FAULT 31
4.3 FAULT LOCATION 35
4.4 FAULT LOCATION FOR SPECIAL CASES 36
4.5 ANALYSES OF THE DG EFFECTS ON THE PROPOSED METHOD 38

5 VALIDATION OF THE PROPOSED METHOD 42

5.1 NUMERICAL PROCEDURE FOR THE FAULT CURRENT CALCULATION 43
5.2 METHOD SENSITIVITY TO THE FAULT RESISTANCE 45
5.3 METHOD SENSITIVITY UNDER UNBALANCED SYSTEM CONDITION 46
5.4 METHOD SENSITIVITY UNDER DIFFERENT LOADING CONDITION 47
5.5 METHOD SENSITIVITY BY CONSIDERING LINE PARAMETER ERRORS 47
5.6 METHOD SENSITIVITY UNDER VOLTAGE MEASUREMENT ERRORS 48
5.7 METHOD SENSITIVITY UNDER DG PRESENCE 49
5.8 METHOD SENSITIVITY TO THE LOAD MODEL VARIATION 53
5.9 SIMULATION RESULTS FOR THE IEEE 69-BUS DISTRIBUTION SYSTEM 53
5.10 SIMULATION RESULTS FOR THE 134-BUS DISTRIBUTION SYSTEM 55

6. DISCUSSIONS AND COMPARISONS 63

6.1 DISCUSSIONS AND COMPARISONS WITH REFERENCE [16] 63
6.2 DISCUSSIONS AND COMPARISONS WITH REFERENCES [10], [17], [18], AND [21] 63

7 CONCLUSIONS 65

REFERENCES 67

1. INTRODUCTION

Significantly reducing restoration time in distribution networks, fault location process improves the quality of the electricity supply for the customers [1]. Due to such benefits, several methods for fault location have been proposed in the literature. The existing methods can be classified into two categories, conventional techniques (traveling wave method and impedance-based method) and artificial intelligence techniques (support vector machine, fuzzy logic, artificial neural network, genetic algorithm, and matching approach) [2].

Since travelling wave methods are more appropriate for transmission lines and artificial intelligence techniques are time-consuming, impedance-based methods are the simplest and most used in distribution networks. However, the accuracy of impedance-based methods can be affected by some factors such as fault types, fault resistance, distributed generation (DG), unbalanced loads, measurements and line parameters errors [2]-[3].

Basically, both conventional and artificial intelligence methods identify the fault location by analyzing information obtained from intelligent electronic devices (IEDs). Impedance methods estimate the fault distance by adopting voltage and current measurements along with the distribution system parameters, such as load data and line section impedance. Besides voltage and current measurements, some artificial intelligence methods have also been proposed by adopting other quantities, such as the status of protective devices and fault indicators (FIs) [3].

FI is a representative intelligent device able to detect the passage of fault current [4]. Smart meters (SMs) are applied to methods that require nonsynchronized measurements of voltage and/or current, while phasor measurement units (PMUs) and digital fault recorders (DFRs) are employed when synchronized measurements of voltage and/or current are required. Due to their cost and the low angle differences of distribution networks, PMUs are commonly employed in transmission systems. However, the recently developed μPMU provides micro-second resolution and millidegree accuracy, which is 100 times the resolution of traditional transmission-type PMU. Therefore, μPMU refers to an excellent tool for fault location in distribution networks [5].

Although IEDs accuracy has improved with the advancement of technology, the robustness and simplicity of fault location methods are directly associated with the number of IEDs installed in the network. Identifying the fault location is a simple task when, for example, pre- and during-fault voltage measurements are available at all buses of the system. However, since it is not a reasonable procedure, most of the fault location techniques have been proposed by considering measuring devices at a few buses. In fact, methods that require all buses equipped with IEDs have their application restricted to active distribution networks, where the whole system is monitored in real-time.

Although providing robust location results with few IEDs is more attractive, it is significantly challenging. To circumvent the lack of information caused by the sparse measurements, some impedance-based methods require load data to calculate the voltage and current at buses without measuring devices. Although such a procedure can be easily performed through classical load flow programs, they are time-consuming. Furthermore, smart load meters and/or state estimation techniques should also be used to obtain load parameters, which further increase the cost and time-consuming, respectively.

In order to reduce the cost and time-consuming, essential during the fault location process, some impedance-based methods have neglected load data, i.e., the impedance matrix is built considering only the line sections impedance. For such methods, the sparse measurements result in underdetermined systems of equations, solved by optimization techniques. In addition to reducing time-consuming, these methods are less exposed to data acquisition errors as fewer parameters are required. On the other hand, the mathematical complexity is significantly increased, resulting in a method less accessible to the utility engineering.

Based on the previous statements, the challenges in proposing a new method for fault location are to obtain it so that the fault location is quickly identified using few IEDs and without mathematical complexity. From this, in this work, an algorithm for fault location in distribution networks is proposed based on a few voltage measurements along with the impedance matrix of the distribution system, where load data is not required. To avoid mathematical complexity, caused by the sparse measurements, a new impedance matrix manipulation procedure is proposed so that the distribution system is investigated in partitions across multiple subsystems. This procedure allows the fault location process to be performed by solving determined systems of equations, which in fact makes the method more technically accessible. Moreover, since the determined systems of equations are solved by a simple multiplication of matrices and vectors, the method provides a computational time of less than three seconds.

2. LITERATURE REVIEW

The fault location algorithm proposed in [6] is one of the primary works of fault location in distribution networks, presenting accurate location results for different fault types and resistances. Such a method requires pre- and during-fault phasors of voltage and current at the substation-bus, during-fault voltage sag magnitude measured at few buses along the feeder, impedance matrix of the distribution system, and the nominal power of all distribution transformers. Pre-fault quantities recorded at the substation-bus are used to calculate the total pre-fault complex power of the feeder, used to estimate the power of each distribution transformer. Through a load flow program, during-fault quantities recorded at the substation-bus are used to calculate the during-fault voltages at buses with measuring devices. By comparing the calculated and measured during-fault voltages, the fault location is identified. Although few measuring devices are required, the method proposed in [6] presents an iterative process using load flows. Furthermore, the method performance is not investigated under noisy measurement conditions.

Similar to [6], the method proposed in [7] also uses phasors of voltage and current at the substation-bus along with the impedance matrix, and voltage measurements are not required along the feeder. Unlike [6], the method proposed in [7] is investigated under voltage measurement errors, where robust location results are achieved for a wide range of fault resistance. However, for single line to ground (LG) faults (most common fault type in distribution systems) the method accuracy is degraded due to the load variations. To improve the method robustness for LG fault, an iterative process is used by adopting pre-fault quantities to calculate the load impedance accordingly, increasing the run time.

A generalized fault location method suitable for distribution systems is presented in [8]. The main purpose of this method is to prevent multiple fault locations from being pinpointed. Moreover, its robustness depends on the accuracy of the source, feeder, and load impedance data and, hence, accurate data should be acquired. Therefore, besides voltage and current measurements, all buses with loads should be equipped with smart load meters capable of providing the load data impedance accurately during the fault location.

A method very similar to [6] is presented in [9]. Pre-fault and during-fault voltage and current phasors at the substation-bus, as well as knowledge about faulted phase(s) and fault type, are utilized. Pre-fault quantities are used to estimate load variations and update load models, while during-fault data are used to pinpoint the fault location. Voltage sags are also gathered from meters installed at some selected buses along the feeder. All buses are assumed as the faulted bus (one at a time) and, through a load flow program, voltage sags are calculated for all buses with voltage measuring devices. Then, the fault location is identified by comparing the calculated voltage sags with the record voltage sags, where the highest similarity indicates the fault location. In this method, there is a time-consuming stage in which the line currents are calculated using a pre-fault load flow. For this, load data should be provided by smart load meters.

The method presented in [10] employs smart feeder meters with voltage sag monitoring capability at a few buses to estimate the fault location in distribution networks. The voltage sags are processed and used to estimate the short-circuit current and, consequently, the fault location. This method requires load data to update the nodal impedance matrix at each iteration. The load data can be obtained in two different ways, using a state estimation technique or installing smart load meters. While the state estimation increases the run time, installing smart load meters for all consumers is costly. Good results are obtained under a wide range of fault resistance and voltage measurement errors. However, the method performance is only evaluated for LG and LLL faults.

A training-based fault location technique for distribution networks is proposed in [11]. Voltage and current phasors measurements are required at the substation-bus, as well as voltage magnitude at few buses along the feeder. However, the algorithm needs power injection metering at all buses with the load to perform pre- and during-fault load flows in different scenarios. One of the main problems related to training-based fault location algorithms is that they need to be retrained after any system reconfiguration to accurately locate the faults, which is a time-consuming and challenging process [2]-[3].

A method for fault location in distribution system with DGs is proposed in [12]. PMUs are deployed at the substation-bus and at all terminal-buses, and the network topology and line parameters must be known. By an iterative process, candidate locations are identified by utilizing the measurement at one terminal-bus. The actual fault location is pinpointed by comparing calculated and measured voltage phasors at junction-buses. When calculating voltage phasors, load data must be known, which would require smart load meters for all consumers.

Also similar to [6], the method proposed in [13] uses voltage and current phasors at the substation, pre- and during-fault voltage magnitude at few buses along the feeder, impedance matrix of the distribution system, and the nominal power of all distribution transformers. By means of a Fuzzy-ARTMAP neural network, the fault type and the phases involved in the fault are identified. The pre-fault quantities recorded at substation-bus are used to calculate the pre-fault apparent power supplied by the feeder, which is used to estimate the distribution transformers load before the instance of the fault occurrence. The fault location is estimated after all voltages and currents are known at all buses as well as the during-fault current at the substation. Unlike [6], the method presented in [13] works with the presence of DG.

In [14], pre- and during-fault voltage and pre-fault current are required at the substation-bus along with the fault level data of each DG unit connected to the distribution network, the fault level data of the substation source, and the apparent power of the distribution transformers. The fault level data are used to calculate the Thevenin equivalents of each source, while the apparent powers of the distribution transformers are used to estimate the impedance of the loads. The fault location is identified through an optimization process that estimates the fault distance in order to minimize the error between the estimated during-fault voltages phasor quantities and the measured ones, increasing the mathematical complexity.

A high-frequency impedance-based fault location technique is proposed in [15] for distribution systems with inverter-interfaced DGs (IIDGs). Voltage and current at a few buses, line section impedance, DG parameters, and load impedance must be known as input data. In addition to the voltage and current measurements, load data must also be provided by IEDs. As a significant number of measuring devices is necessary, the cost of implementation of the method is high. Moreover, this method cannot be used to locate high impedance faults and ground faults.

The method proposed in [16] is developed based on a negative sequence analysis. Thus, since conventional inverters applied to DGs normally use eliminating negative sequence control, this method is less affected by IIDGs. For such a method, sparse voltage measurements along with the distribution system impedance matrix must be known. Also, all consumers should be equipped with IEDs capable of providing load data at the exact moment of the fault. As the fault is located investigating only the negative sequence component, this method does not work for LLL fault, where the fault current consists only of the positive sequence.

Although similar input data are required in [6]-[16], the methods proposed in [6]-[11] cannot be applied to distribution networks with DG. In [6]-[16], state estimation techniques or smart load meters are required to obtain load data. While state estimation techniques increase the run time, methods that require smart load meters for all consumers are restricted to active distribution systems. After estimating the loads data, pre- and/or during-fault voltages must also be estimated along the feeder. Due to the multiple estimation stages, such methods are time-consuming and may not converge at some stage due to measurement errors. As many different quantities must be acquired, such as voltage, current, load, line section impedance, and DG data, these methods are more subject to data acquisition errors.

SMs or PMUs can be placed at a few buses of the distribution system to measure pre-fault and during-fault voltages in [17] and [18]. The voltage sags of all buses with meters are used to produce a voltage sag vector, with dimensions lower than the number of buses in the network. The nodal impedance matrix and the voltage sag vector are used to compose an underdetermined system of equations that is formulated by a compressive sensing technique and solved by primal-dual interior-point, resulting in a current sparse vector. The method proposed in [17] is able to locate simultaneous fault by using the k-nearest neighborhood technique to estimate a single fault location, while in [18] the higher value of the current sparse vector indicates the faulted bus. Both methods, [17] and [18], may be technically and economically more attractive than [7]-[11], as the loads impedance are not considered in the impedance matrix.

The fault location methods proposed in [17] and [18] present accurate results for any fault type and fault impedance value by employing only 9 to 22 measuring devices in a 134-bus system. However, in both methods, there is no technique showing guidelines on where measurement devices should be installed, and the presence of DG is not addressed. In addition, the effect of PMUs accuracy on a compressive sensing-based fault location algorithm has been studied and discussed by means of simulations in [19]. The results show how the compressive sensing technique is subject to significant performance degradation under more realistic uncertainties.

In [20], the faulted area of the distribution system is identified based on the voltage measurements provided by SMs. In fact, such a method is used to improve the performance of conventional impedance-based techniques, identifying the area where the voltage magnitude is low due to the proximity of fault location. Although few SMs are required, such a method is not evaluated in a scenario with DG.

The method proposed in [21] considers important issues not addressed by previous methods presented in [17], [18], and [20]. This method is capable to estimate faults in distribution networks with or without the presence of any type of DG. For this, synchronized and nonsynchronized measurements are required at a few buses. The voltage sag at buses with DG must be measured synchronously, while it is not necessary for buses without DG. As a μPMU must be installed for each DG, this method may become economically unfeasible for systems with several DG units.

In [22], digital fault recorders (DFRs) are placed at the substation source and at the coupling point of each DG unit (one DG must be installed at the last bus of the distribution system). By considering the waveforms as synchronized phasors, it is possible to obtain the fault current value through the sum of the currents injected by each DG and the substation source. Knowing the nodal impedance matrix of the system with N buses, $N + d$ different voltages drops are calculated in all buses with DG (d corresponds to the number of fictitious buses created in sections between actual buses). Since the actual voltage drop in each bus with DG is measured, the calculated voltage sag presenting lower error compared to the actual voltage drop corresponds to the location of the fault. As it is necessary to place a DFR for each DG, the implementation cost of such a method may become expensive for systems with high DG penetration. Furthermore, the fault current contributions of DGs may not be reliable due to CT saturation and errors, and this method may identify the fault at different laterals with the same impedance.

The method proposed in [23] assumes that pre- and during-fault synchronized measurements of voltages and currents are also obtained from DFRs at the substation and at each DG unit. The pre-fault data are used to estimate the load power demand at each bus of the system through a load-flow, increasing the run time. Unlike [22], where the DG units are inserted as impedance into the nodal matrix, DGs are adopted as current sources in [23]. The impedance matrix and the during-fault voltages are used to identify the fault location. This method also locates the faults regardless of DG type and interface, but can also be affected by CT saturation and errors.

A PMU based fault detection and location method for distribution networks using real-time state estimation is presented in [24]. The method estimates the faulted line regardless of the type and number of DGs, fault type, and fault impedance value. Nevertheless, PMUs must be installed at all buses of the distribution system, which can be seen as a problem from the economic point of view.

The methods proposed in [25]-[26] identify the faulted section in distribution networks with/without DGs by employing fault indicators (FIs). Although load data are not required, a considerable number of FIs must be placed for such methods. In addition to installing FIs, some buses of the distribution system must also be equipped with SMs for the method proposed in [27]. Even adopting eight SMs and seven FIs for the IEEE 33-bus test feeder, the method proposed in [27] is not capable to pinpoint the exact point of the fault. In fact, only the faulted lateral can be identified.

Based on the review described previously, this work introduces a new method for fault location in distribution networks with significant contributions, as follows:

- Compared to [6]-[16], the proposed method does not require loads data. Only the voltage sag at a few buses and the impedance matrix must be known.
- Unlike [8], [10], [15], and [16], all fault types are considered in the proposed method with a wide range of fault resistance.
- The present method provides accurate location results for systems with/without DG, regardless of the DG type. In [6]-[11], [17], [18], and [20] DGs are not introduced, and only IIDGs are addressed in [15] and [16].
- The proposed method requires only two μPMUs and few SMs for whatever the system size resulting in fewer IEDs in general than [8]-[12], [15], [16], and [24]-[27].
- Unlike [6], [8], [22], and [23], the present method is evaluated by considering errors for the measuring devices (measurement errors) and for the impedance matrix.
- For the methods described in [21]-[23], additional synchronized measuring devices must be installed when new DG units are connected, which is not necessary for the method proposed in this work.
- The present method locates the fault without mathematical complexity. Determined systems of equations are solved by a simple multiplication of matrices and vectors. Thus, besides being a method more accessible to the utility professionals, it provides a computational time of less than three seconds.

3. CLASSICAL FAULT CURRENT CALCULATION

This section is dedicated to discussing a classical method for fault current calculation using voltage sag measurements along with the distribution system impedance matrix. Since the pre- and during-fault voltages recorded by measuring devices already contemplate the loads effects, the system impedance matrix can be built considering only the impedance of the line sections [18].

3.1 FAULT CURRENT CALCULATION CONSIDERING MEASURING DEVICES AT ALL BUSES

Initially, the fault current calculation process is presented assuming all buses equipped with μPMUs capable of providing synchronized pre- and during-fault voltages. For simplicity, the 8-bus distribution system of Figure 1 is adopted. All line sections are considered with the same three-phase impedance Z, and Z_T is the three-phase impedance of the substation transformer. Such a transformer is represented by a primitive impedance matrix with 3x3 dimension, composed by the self and mutual impedances of the windings, regardless of their connection type.

Figure 1 - 8-bus distribution system under fault condition at bus-6

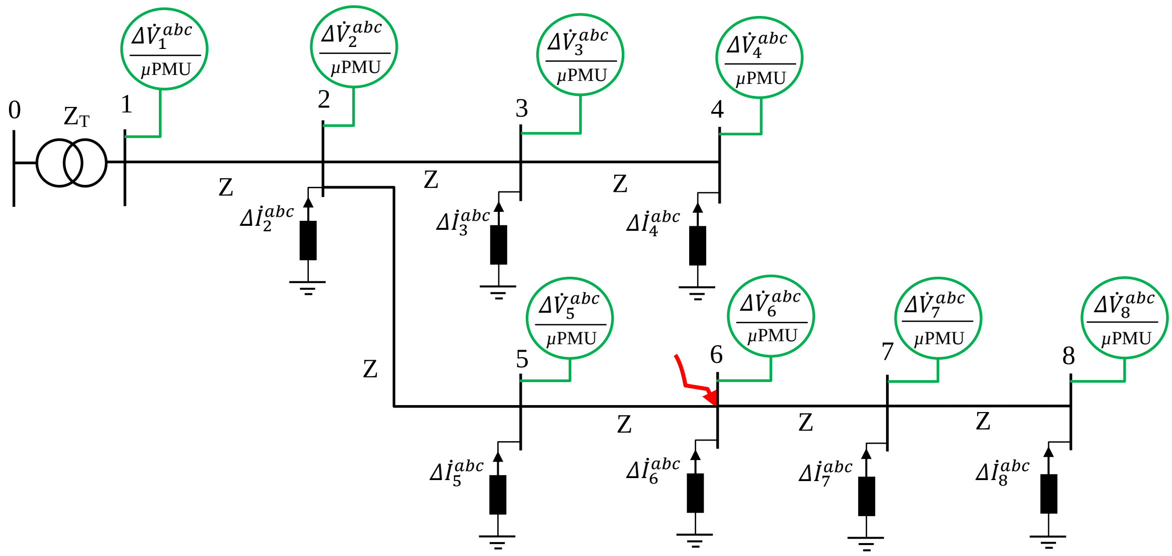

Source: Authors

When a fault occurs at bus-6 of the 8-bus distribution system of Figure 1, for example, the synchronized pre- and during-fault voltages can be recorded from all μPMUs. Thus, pre- and during-fault voltages can be used to calculate the voltage sag at each bus, as (1), where $\dot{V}_n^{abc,pf}$ and $\dot{V}_n^{abc,f}$ are, respectively, the three-phase pre- and during-fault voltages at bus-n.

$$\Delta\dot{V}_n^{abc} = \begin{bmatrix} \dot{V}_n^{a,pf} \\ \dot{V}_n^{b,pf} \\ \dot{V}_n^{c,pf} \end{bmatrix}_{3x1} - \begin{bmatrix} \dot{V}_n^{a,f} \\ \dot{V}_n^{b,f} \\ \dot{V}_n^{c,f} \end{bmatrix}_{3x1} \tag{1}$$

After calculating the voltage sag for all buses, a voltage sag vector can be defined. By multiplying the inverse of the impedance matrix of the distribution system by the voltage sag vector, a current sparse vector is obtained. As the fault current is significantly higher than the variation of the pre- and during-fault current of the loads, the current sparse vector has one nonzero element, as described in (2).

$$\begin{bmatrix} 0 \\ 0 \\ 0 \\ 0 \\ 0 \\ -\dot{I}_6^{abc} \\ 0 \\ 0 \end{bmatrix}_{24x1} = inv \begin{bmatrix} Z_T & Z_T & Z_T & Z_T & Z_T & Z_T & Z_T & Z_T \\ Z_T & Z_T+Z & Z_T+Z & Z_T+Z & Z_T+Z & Z_T+Z & Z_T+Z & Z_T+Z \\ Z_T & Z_T+Z & Z_T+2Z & Z_T+2Z & Z_T+Z & Z_T+Z & Z_T+Z & Z_T+Z \\ Z_T & Z_T+Z & Z_T+2Z & Z_T+3Z & Z_T+Z & Z_T+Z & Z_T+Z & Z_T+Z \\ Z_T & Z_T+Z & Z_T+Z & Z_T+Z & Z_T+2Z & Z_T+2Z & Z_T+2Z & Z_T+2Z \\ Z_T & Z_T+Z & Z_T+Z & Z_T+Z & Z_T+2Z & Z_T+3Z & Z_T+3Z & Z_T+3Z \\ Z_T & Z_T+Z & Z_T+Z & Z_T+Z & Z_T+2Z & Z_T+3Z & Z_T+4Z & Z_T+4Z \\ Z_T & Z_T+Z & Z_T+Z & Z_T+Z & Z_T+2Z & Z_T+3Z & Z_T+4Z & Z_T+5Z \end{bmatrix}_{24x24} \cdot \begin{bmatrix} \Delta\dot{V}_1^{abc} \\ \Delta\dot{V}_2^{abc} \\ \Delta\dot{V}_3^{abc} \\ \Delta\dot{V}_4^{abc} \\ \Delta\dot{V}_5^{abc} \\ \Delta\dot{V}_6^{abc} \\ \Delta\dot{V}_7^{abc} \\ \Delta\dot{V}_8^{abc} \end{bmatrix}_{24x1} \tag{2}$$

The nonzero element of the current sparse vector refers to the fault current, where its position indicates the faulted bus. The fault current ($\dot{I}_f^{abc}$=$\dot{I}_6^{abc}$) has one nonzero value, two nonzero values, and three nonzero values for single-phase, double-phase, and three-phase faults, respectively [18].

In (2), it can be noted that the voltage sags at all buses are caused only by the fault current (all other elements are zero). In fact, the current vector only results with one nonzero element if and only if the pre- and during-fault currents of the loads are identical, which is only true if the loads operate as “constant current model”. However, although most of the loads in distribution networks operate as “constant power model”, the load current variation is significantly lower than the fault current value. Therefore, applying the voltage sag concept means to assume that the pre- and during-fault current variation of the loads is negligible when compared to the fault current.

The premise described in (2) is executable since the voltage sag is known at the exact point of the fault, i.e., when a fault occurs on a bus. To demonstrate how the fault current and the fault location are obtained when a fault occurs in a section, the 8-bus distribution system is illustrated in Figure 2 under fault condition in section 5-6.

Figure 2 – 8-bus distribution system under fault condition at section 5-6

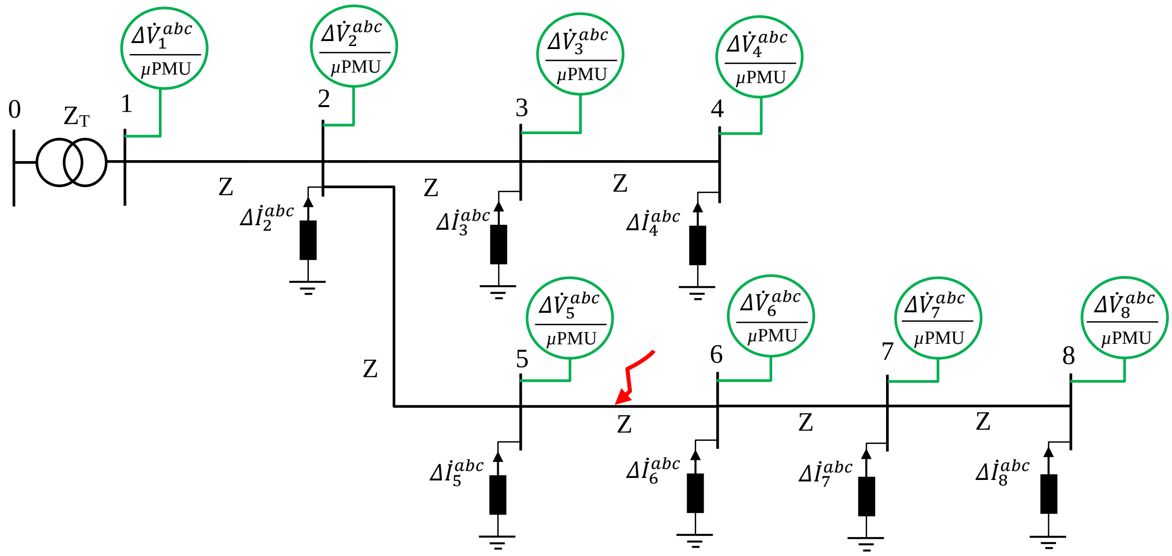

Source: Authors

When a fault occurs at section 5-6, the same procedure in (2) is carried out. However, as can be seen in (3), two nonzero elements arise in the current sparse vector due to the lack of a measuring device at the exact point of the fault. The positions of the nonzero elements indicate the upstream and downstream buses closest to the fault location. Therefore, the positions of the nonzero elements in (3) indicate that the fault occurred between buses 5 and 6.

$$\begin{bmatrix} 0 \\ 0 \\ 0 \\ 0 \\ -\dot{I}_5^{abc} \\ -\dot{I}_6^{abc} \\ 0 \\ 0 \end{bmatrix}_{24x1} = inv \begin{bmatrix} Z_T & Z_T & Z_T & Z_T & Z_T & Z_T & Z_T & Z_T \\ Z_T & Z_T+Z & Z_T+Z & Z_T+Z & Z_T+Z & Z_T+Z & Z_T+Z & Z_T+Z \\ Z_T & Z_T+Z & Z_T+2Z & Z_T+2Z & Z_T+Z & Z_T+Z & Z_T+Z & Z_T+Z \\ Z_T & Z_T+Z & Z_T+2Z & Z_T+3Z & Z_T+Z & Z_T+Z & Z_T+Z & Z_T+Z \\ Z_T & Z_T+Z & Z_T+Z & Z_T+Z & Z_T+2Z & Z_T+2Z & Z_T+2Z & Z_T+2Z \\ Z_T & Z_T+Z & Z_T+Z & Z_T+Z & Z_T+2Z & Z_T+3Z & Z_T+3Z & Z_T+3Z \\ Z_T & Z_T+Z & Z_T+Z & Z_T+Z & Z_T+2Z & Z_T+3Z & Z_T+4Z & Z_T+4Z \\ Z_T & Z_T+Z & Z_T+Z & Z_T+Z & Z_T+2Z & Z_T+3Z & Z_T+4Z & Z_T+5Z \end{bmatrix}_{24x24} \cdot \begin{bmatrix} \Delta\dot{V}_1^{abc} \\ \Delta\dot{V}_2^{abc} \\ \Delta\dot{V}_3^{abc} \\ \Delta\dot{V}_4^{abc} \\ \Delta\dot{V}_5^{abc} \\ \Delta\dot{V}_6^{abc} \\ \Delta\dot{V}_7^{abc} \\ \Delta\dot{V}_8^{abc} \end{bmatrix}_{24x1} \quad (3)$$

In this case, the fault current is given by the sum of both nonzero elements of the current sparse vector, as (4).

$$\dot{I}_f^{abc} = \dot{I}_5^{abc} + \dot{I}_6^{abc} \quad (4)$$

In addition to locating the faulted section correctly, the exact point of the fault can also be identified. For this, the faulted section 5-6 is illustrated in Figure 3 under three different fault locations, where l_1, l_2, and l_3 are the distances between the upstream bus (bus-5) and the fault locations F_1, F_2, and F_3, respectively. Such distances are given by the section length percentage.

Figure 3 – Section 2-3 under three different fault scenarios

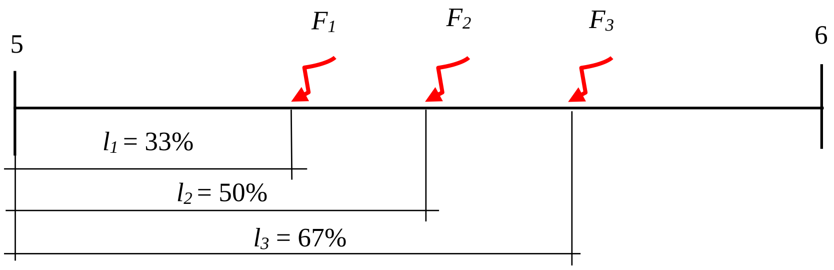

Source: Authors

Equation (4) is valid regardless of the fault location in section 5-6. However, as described in (5) and (6), the values of $\dot{I}_5^{abc}$ and $\dot{I}_6^{abc}$ vary according to the fault location, where l_i is the distance between the upstream bus (bus-5) and the fault locations F_i. Therefore, the fault distance can be calculated from (5) or (6). It can also be noted that $\dot{I}_5^{abc} = \dot{I}_6^{abc}$ when a fault occurs exactly in the middle of section 5-6 (Fault F_2 in Figure 3).

$$\dot{I}_5^{abc} = \frac{\dot{I}_f^{abc} \cdot l_i}{100} \tag{5}$$

$$\dot{I}_6^{abc} = \frac{\dot{I}_f^{abc} \cdot \left(100 - l_i\right)}{100} \tag{6}$$

In order to show that the fault current can be calculated from (3) to (6), data are assigned to the 8-bus system of Figure 2 on DIgSILENT software [28]. A 500kVA, 69/13.8kV three-phase power transformer is placed at the substation with a resistance of 1% and a reactance of 3%. All line sections are adopted with 100 meters and with the primitive impedance matrix of Table 1. At all buses, a load of 70 kW is placed as a “constant power model”.

Table 1 – Primitive impedance matrix (ohm/km) applied to all sections of the 8-bus system.

0.8265 + j0.8364	0.1305 + j0.3187	0.1305 + j0.3187
0.1305 + j0.3187	0.8265 + j0.8364	0.1305 + j0.3187
0.1305 + j0.3187	0.1305 + j0.3187	0.8265 + j0.8364

Source: Data of the author

When a three-phase fault (LLL) occurs at 50% of section 5-6 with a fault resistance of 100 ohms, (3) results as (7). For simplicity, the magnitude of the resulting current vector residuals is presented.

$$\begin{bmatrix} 0.85 \\ 2.96 \\ 1.62 \\ 0.97 \\ \mathbf{37.62\angle{-7.38}^\circ} \\ \mathbf{37.59\angle{-8.50}^\circ} \\ 0.38 \\ 0.38 \end{bmatrix}_{24x1} = inv \begin{bmatrix} Z_T & Z_T & Z_T & Z_T & Z_T & Z_T & Z_T & Z_T \\ Z_T & Z_T+Z & Z_T+Z & Z_T+Z & Z_T+Z & Z_T+Z & Z_T+Z & Z_T+Z \\ Z_T & Z_T+Z & Z_T+2Z & Z_T+2Z & Z_T+Z & Z_T+Z & Z_T+Z & Z_T+Z \\ Z_T & Z_T+Z & Z_T+2Z & Z_T+3Z & Z_T+Z & Z_T+Z & Z_T+Z & Z_T+Z \\ Z_T & Z_T+Z & Z_T+Z & Z_T+Z & Z_T+2Z & Z_T+2Z & Z_T+2Z & Z_T+2Z \\ Z_T & Z_T+Z & Z_T+Z & Z_T+Z & Z_T+2Z & Z_T+3Z & Z_T+3Z & Z_T+3Z \\ Z_T & Z_T+Z & Z_T+Z & Z_T+Z & Z_T+2Z & Z_T+3Z & Z_T+4Z & Z_T+4Z \\ Z_T & Z_T+Z & Z_T+Z & Z_T+Z & Z_T+2Z & Z_T+3Z & Z_T+4Z & Z_T+5Z \end{bmatrix}_{24x24} \cdot \begin{bmatrix} \Delta\dot{V}_1^{abc} \\ \Delta\dot{V}_2^{abc} \\ \Delta\dot{V}_3^{abc} \\ \Delta\dot{V}_4^{abc} \\ \Delta\dot{V}_5^{abc} \\ \Delta\dot{V}_6^{abc} \\ \Delta\dot{V}_7^{abc} \\ \Delta\dot{V}_8^{abc} \end{bmatrix}_{24x1} \tag{7}$$

From (4) to (7), it can be verified that a fault occurred exactly at 50% of section 5-6, with a fault current value of 75.32 A. As discussed previously, even operating as “constant power model”, the loads current variation is negligible when compared to the fault current. For comparative purposes, the fault current obtained in DIgSILENT is 75.15 A.

3.2 FAULT CURRENT CALCULATION REDUCING THE NUMBER OF MEASURING DEVICES

As described in item 3.1, calculating the fault current and identifying the fault location is a simple task when voltage measurements are known at all buses of the distribution system. However, installing measuring devices at all buses is not a reasonable solution. For this, in order to reduce the number of measuring devices, μPMUs are considered only at the substation-bus (bus-1), terminal-buses (bus-4 and bus-8), and junction-buses (bus-2) as shown in Figure 4.

Figure 4 – 8-bus distribution system with a reduced number of μPMUs

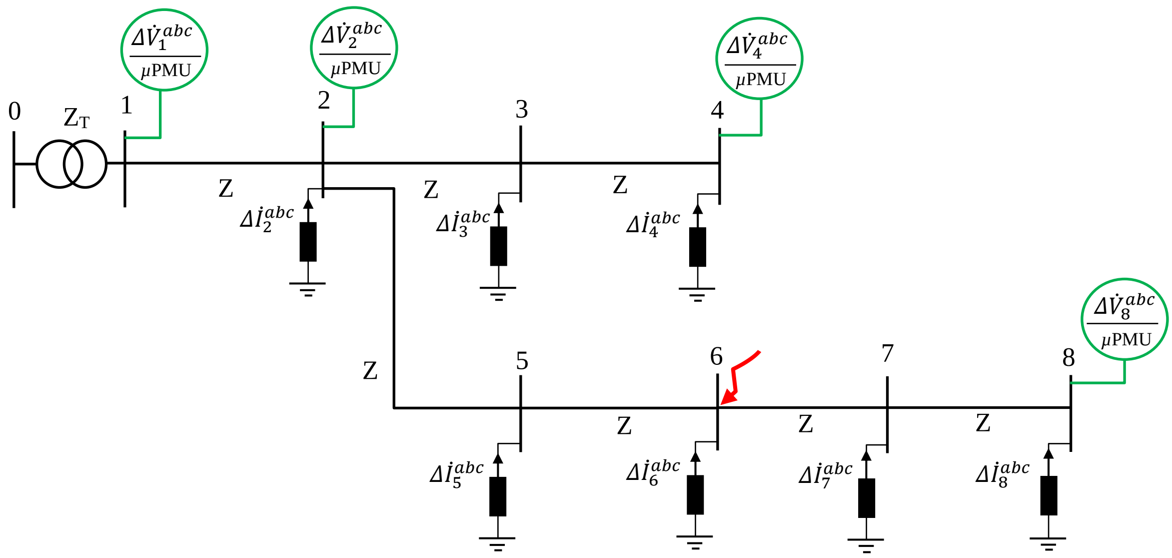

Source: Authors

From Figure 4, it is verified that the number of measuring devices is lower than the number of buses, i.e., voltage measurements cannot be recorded at all buses. Even under such a scenario, when a fault occurs at bus-6, the fault current can be calculated without requiring load data, load flow programs, and optimization techniques. For this, the impedance matrix must be built by eliminating the buses without measuring devices as illustrated in Figure 5.

Figure 5 – 8-bus distribution system without buses 3, 5, 6, and 7

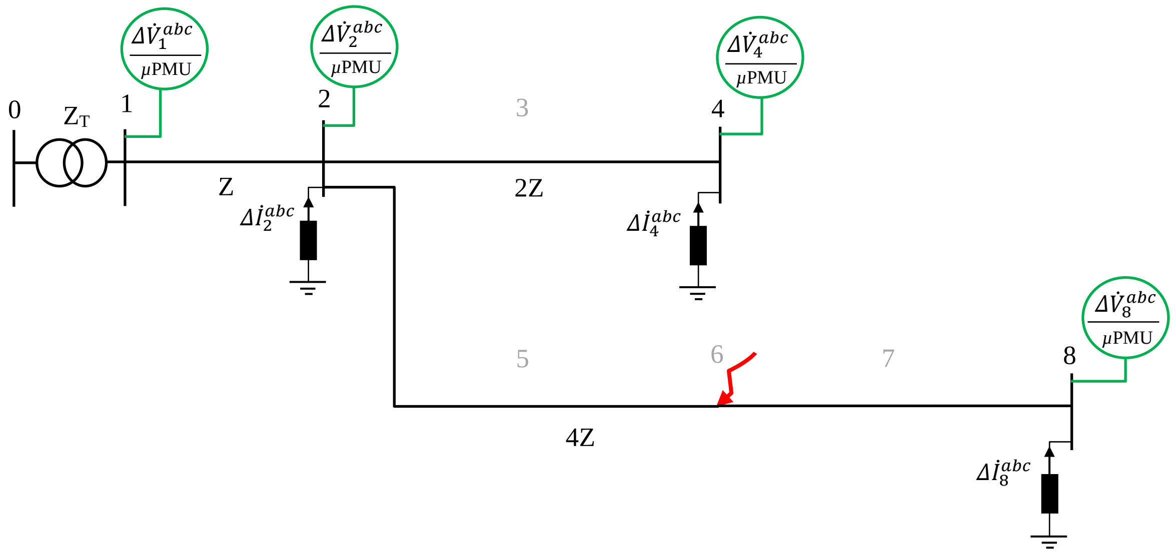

Source: Authors

As illustrated in Figure 5, buses 3, 5, 6, and 7 are eliminated. However, the series impedance between the substation-bus and all terminal-buses does not change, i.e., the series impedance between bus-1 and bus-8, for example, is 5Z for both topologies shown in Figure 4 and Figure 5. Therefore, by assuming the topology in figure 5, the fault current is calculated by (8) and (9).

$$\begin{bmatrix} 0 \\ -\dot{I}_2^{abc} \\ 0 \\ -\dot{I}_8^{abc} \end{bmatrix}_{12x1} = inv \begin{bmatrix} Z_T & Z_T & Z_T & Z_T \\ Z_T & Z_T+Z & Z_T+Z & Z_T+Z \\ Z_T & Z_T+Z & Z_T+3Z & Z_T+Z \\ Z_T & Z_T+Z & Z_T+Z & Z_T+5Z \end{bmatrix}_{12x12} \cdot \begin{bmatrix} \Delta\dot{V}_1^{abc} \\ \Delta\dot{V}_2^{abc} \\ \Delta\dot{V}_4^{abc} \\ \Delta\dot{V}_8^{abc} \end{bmatrix}_{12x1} \tag{8}$$

$$\dot{I}_f^{abc} = \dot{I}_2^{abc} + \dot{I}_8^{abc} \tag{9}$$

Even reducing the number of voltage measurements, the adopted procedure allows the fault current to be correctly calculated from a determined system of equations. The nonzero elements of the current sparse vector, in (7), indicate that the fault occurred between buses 2 and 8. Furthermore, since the fault current is significantly higher than the variation of the pre- and during-fault current of the eliminated loads at buses 3, 5, 6, and 7, the fault distance can also be calculated by (5) or (6).

In order to verify the procedure described in (8) and (9) through numerical analysis, a LLL fault is simulated at bus-6, in DIgSILENT, with a fault resistance of 100 ohms. By assuming the concept described in (8), the current vector results as indicated in (10).

$$\begin{bmatrix} 0.24 \\ \mathbf{37.40\angle\text{-}9.53^\circ} \\ 0.48 \\ \mathbf{37.25\angle\text{-}9.10^\circ} \end{bmatrix}_{12x1} = inv\begin{bmatrix} Z_T & Z_T & Z_T & Z_T \\ Z_T & Z_T+Z & Z_T+Z & Z_T+Z \\ Z_T & Z_T+Z & Z_T+3Z & Z_T+Z \\ Z_T & Z_T+Z & Z_T+Z & Z_T+5Z \end{bmatrix}_{12x12} \cdot \begin{bmatrix} \Delta\dot{V}_1^{abc} \\ \Delta\dot{V}_2^{abc} \\ \Delta\dot{V}_4^{abc} \\ \Delta\dot{V}_8^{abc} \end{bmatrix}_{12x1} \quad (10)$$

From (5), (6), (9), and (10), it can be verified that the fault occurred at 50% of section 2-8 with a fault current value of 74.65 A. In Figures 4 and 5, it can be seen that bus-6 is located exactly at 50% of section 2-8. The fault current obtained in DIgSILENT is 75.12 A, allowing to verify the accuracy of the analyzed concept.

3.3 FAULT CURRENT CALCULATION UNDER DG PRESENCE

Initially, all buses are equipped with measuring devices, a DG is placed at bus-7, and a fault is considered at 50% of section 5-6, as illustrated in Figure 6.

Figure 6 – 8-bus distribution system with DG at bus-7

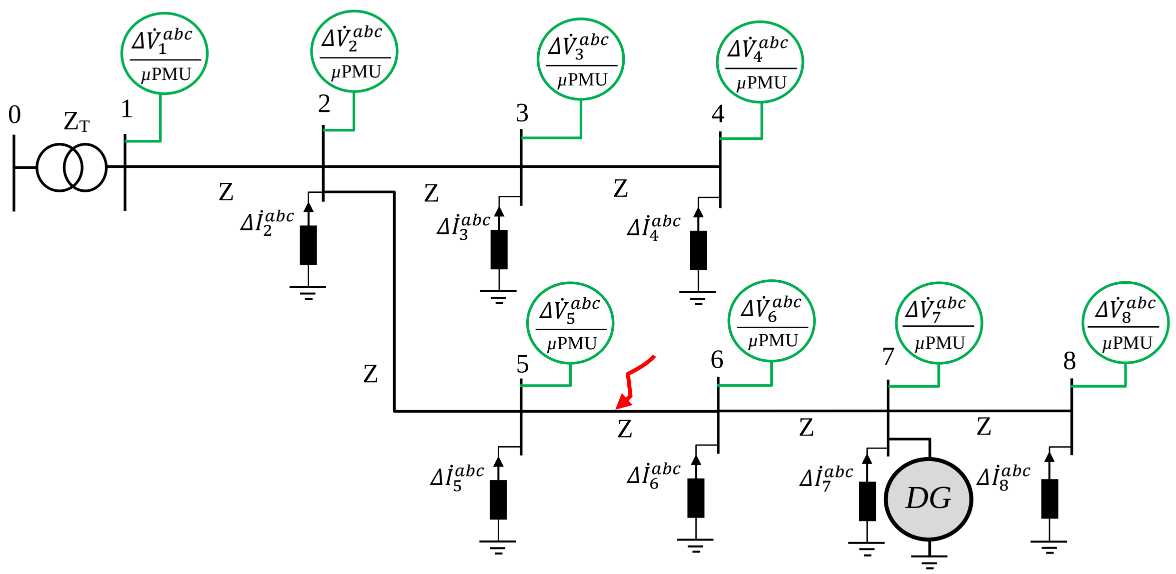

Source: Authors

Under DG presence, (3) is rewritten as (11), where a nonzero element arises at the position of the bus with DG. As indicated in (11), the nonzero element refers to the variation of the pre- and during-fault currents of the DG.

$$\begin{bmatrix} 0 \\ 0 \\ 0 \\ 0 \\ -\dot{I}_5^{abc} \\ -\dot{I}_6^{abc} \\ \Delta\dot{I}_7^{abc,DG} \\ 0 \end{bmatrix}_{24x1} = inv\begin{bmatrix} Z_T & Z_T & Z_T & Z_T & Z_T & Z_T & Z_T & Z_T \\ Z_T & Z_T+Z & Z_T+Z & Z_T+Z & Z_T+Z & Z_T+Z & Z_T+Z & Z_T+Z \\ Z_T & Z_T+Z & Z_T+2Z & Z_T+2Z & Z_T+Z & Z_T+Z & Z_T+Z & Z_T+Z \\ Z_T & Z_T+Z & Z_T+2Z & Z_T+3Z & Z_T+Z & Z_T+Z & Z_T+Z & Z_T+Z \\ Z_T & Z_T+Z & Z_T+Z & Z_T+Z & Z_T+2Z & Z_T+2Z & Z_T+2Z & Z_T+2Z \\ Z_T & Z_T+Z & Z_T+Z & Z_T+Z & Z_T+2Z & Z_T+3Z & Z_T+3Z & Z_T+3Z \\ Z_T & Z_T+Z & Z_T+Z & Z_T+Z & Z_T+2Z & Z_T+3Z & Z_T+4Z & Z_T+4Z \\ Z_T & Z_T+Z & Z_T+Z & Z_T+Z & Z_T+2Z & Z_T+3Z & Z_T+4Z & Z_T+5Z \end{bmatrix}_{24x24} \cdot \begin{bmatrix} \Delta\dot{V}_1^{abc,DG} \\ \Delta\dot{V}_2^{abc,DG} \\ \Delta\dot{V}_3^{abc,DG} \\ \Delta\dot{V}_4^{abc,DG} \\ \Delta\dot{V}_5^{abc,DG} \\ \Delta\dot{V}_6^{abc,DG} \\ \Delta\dot{V}_7^{abc,DG} \\ \Delta\dot{V}_8^{abc,DG} \end{bmatrix}_{24x1} \quad (11)$$

In order to verify the procedure described in (11) through numerical analysis, a LLL fault is simulated at 50% of section 5-6 with a fault resistance of 100 ohms, in DIgSILENT, when a synchronous DG with 500 kVA is placed at bus-7. Thus, (11) results as (12).

$$\begin{bmatrix} 0.72 \\ 2.65 \\ 1.48 \\ 0.89 \\ \mathbf{38.39\angle\text{-}4.98^\circ} \\ \mathbf{38.46\angle\text{-}6.02^\circ} \\ \mathbf{10.64\angle 158.26^\circ} \\ 0.29 \end{bmatrix}_{24x1} = inv\begin{bmatrix} Z_T & Z_T & Z_T & Z_T & Z_T & Z_T & Z_T & Z_T \\ Z_T & Z_T+Z & Z_T+Z & Z_T+Z & Z_T+Z & Z_T+Z & Z_T+Z & Z_T+Z \\ Z_T & Z_T+Z & Z_T+2Z & Z_T+2Z & Z_T+Z & Z_T+Z & Z_T+Z & Z_T+Z \\ Z_T & Z_T+Z & Z_T+2Z & Z_T+3Z & Z_T+Z & Z_T+Z & Z_T+Z & Z_T+Z \\ Z_T & Z_T+Z & Z_T+Z & Z_T+Z & Z_T+2Z & Z_T+2Z & Z_T+2Z & Z_T+2Z \\ Z_T & Z_T+Z & Z_T+Z & Z_T+Z & Z_T+2Z & Z_T+3Z & Z_T+3Z & Z_T+3Z \\ Z_T & Z_T+Z & Z_T+Z & Z_T+Z & Z_T+2Z & Z_T+3Z & Z_T+4Z & Z_T+4Z \\ Z_T & Z_T+Z & Z_T+Z & Z_T+Z & Z_T+2Z & Z_T+3Z & Z_T+4Z & Z_T+5Z \end{bmatrix}_{24x24} \cdot \begin{bmatrix} \Delta\dot{V}_1^{abc,DG} \\ \Delta\dot{V}_2^{abc,DG} \\ \Delta\dot{V}_3^{abc,DG} \\ \Delta\dot{V}_4^{abc,DG} \\ \Delta\dot{V}_5^{abc,DG} \\ \Delta\dot{V}_6^{abc,DG} \\ \Delta\dot{V}_7^{abc,DG} \\ \Delta\dot{V}_8^{abc,DG} \end{bmatrix}_{24x1} \quad (12)$$

From (5), (6), (9), and (12), it can be verified that the fault occurred at 50% of section 5-6 with a fault current value of 76.50 A. In DIgSILENT, the magnitude of the resulting fault current is 76.84. In other words, the resulting current vector in (12) indicates that the voltage sag at all buses of the 8-bus system is caused by a punctual fault current injection of 76.50 A at 50% of section 5-6 and by the DG contribution of 10.64 A at bus-7.

Now, in order to verify the DG effects when the number of measuring devices is reduced, the system topology of Figure 5 is adopted. In this analysis, buses 3, 5, 6, and 7 are eliminated. It must be highlighted that bus-7 is eliminated even with the DG presence. Therefore, using only the voltage sag measurements at buses 1, 2, 4, and 8 the current vector results as (13) when a fault occurs at bus-6.

$$\begin{bmatrix} 0.27 \\ \mathbf{35.63\angle -5.54^\circ} \\ 0.44 \\ \mathbf{30.65\angle -2.26^\circ} \end{bmatrix}_{12x1} = inv\begin{bmatrix} Z_T & Z_T & Z_T & Z_T \\ Z_T & Z_T+Z & Z_T+Z & Z_T+Z \\ Z_T & Z_T+Z & Z_T+3Z & Z_T+Z \\ Z_T & Z_T+Z & Z_T+Z & Z_T+5Z \end{bmatrix}_{12x12} \cdot \begin{bmatrix} \Delta\dot{V}_1^{abc,DG} \\ \Delta\dot{V}_2^{abc,DG} \\ \Delta\dot{V}_4^{abc,DG} \\ \Delta\dot{V}_8^{abc,DG} \end{bmatrix}_{12x1} \quad (13)$$

From (5) and (6), the resulting current vector, in (13), indicates that the voltage sags at buses 1, 2, 4, and 8 are caused by a punctual fault current injection of 66.28 A at 46.25% of section 2-8 (Figure 5). In fact, the fault occurred at 50% of section 2-8 (at bus-6). Therefore, a very low error of 3.75% is achieved. In DIgSILENT, a fault current of 76.83 A and DG current variation of 10.05 A are obtained. Therefore, from these analyses, it can be approximately assumed that a unique fault current injection of 66.28 A at bus-6 cause the same voltage sags as a fault current injection of 76.83 A at bus-6 along with a current injection of 10.05 A at bus-7.

Finally, (14) is obtained when the synchronous DG of 500 kVA is placed at bus-5 instead of bus-7. From (13), it is concluded that when the DG is located downstream from the fault, the error tends to indicate points upstream, and the opposite is verified in (14).

$$\begin{bmatrix} 0.31 \\ \mathbf{30.57\angle -2.53^\circ} \\ 0.44 \\ \mathbf{35.66\angle -5.37^\circ} \end{bmatrix}_{12x1} = inv\begin{bmatrix} Z_T & Z_T & Z_T & Z_T \\ Z_T & Z_T+Z & Z_T+Z & Z_T+Z \\ Z_T & Z_T+Z & Z_T+3Z & Z_T+Z \\ Z_T & Z_T+Z & Z_T+Z & Z_T+5Z \end{bmatrix}_{12x12} \cdot \begin{bmatrix} \Delta\dot{V}_1^{abc,DG} \\ \Delta\dot{V}_2^{abc,DG} \\ \Delta\dot{V}_4^{abc,DG} \\ \Delta\dot{V}_8^{abc,DG} \end{bmatrix}_{12x1} \quad (14)$$

Although measuring devices must be installed at substation-bus, junction-buses, and terminal-buses, the investment may still be high. Therefore, to further reduce the implementation cost, this work proposes a method that calculates the fault current without the need for voltage measurements at the junction-buses, which is possible through an impedance matrix manipulation procedure that creates multiple subsystems.

4. PROPOSED METHOD FOR FAULT LOCATION

The proposed method locates the fault based on the formation of multiple subsystems. During the fault location process, each subsystem is investigated separately. Basically, the subsystems represent the laterals of the distribution system. Thus, the number of subsystems to be created is equal to the number of terminal-buses, where each subsystem consists of the series impedance between the substation-bus and its terminal-bus. As illustrated in Figure 7 (b), three subsystems are created for the distribution system of Figure 7 (a). All line sections are considered with the same three-phase impedance Z, and Z_T is the three-phase impedance of the substation transformer.

Regardless of the distribution system size, the proposed method requires only two synchronized voltage measurements and *S*-1 non-synchronized voltage measurements, where *S* is the number of subsystems to be created. As indicated in Figure 7, the synchronized and non-synchronized voltage measurements are represented by μPMUs and SMs, respectively. A μPMU is installed at the substation-bus (or other IED that can provide synchronized measurements, such as digital relays) and at any terminal-bus. Nonsynchronized measuring devices are installed at the remaining terminal-buses.

Figure 7 – (a) 7-bus distribution system; (b) Proposed subsystems

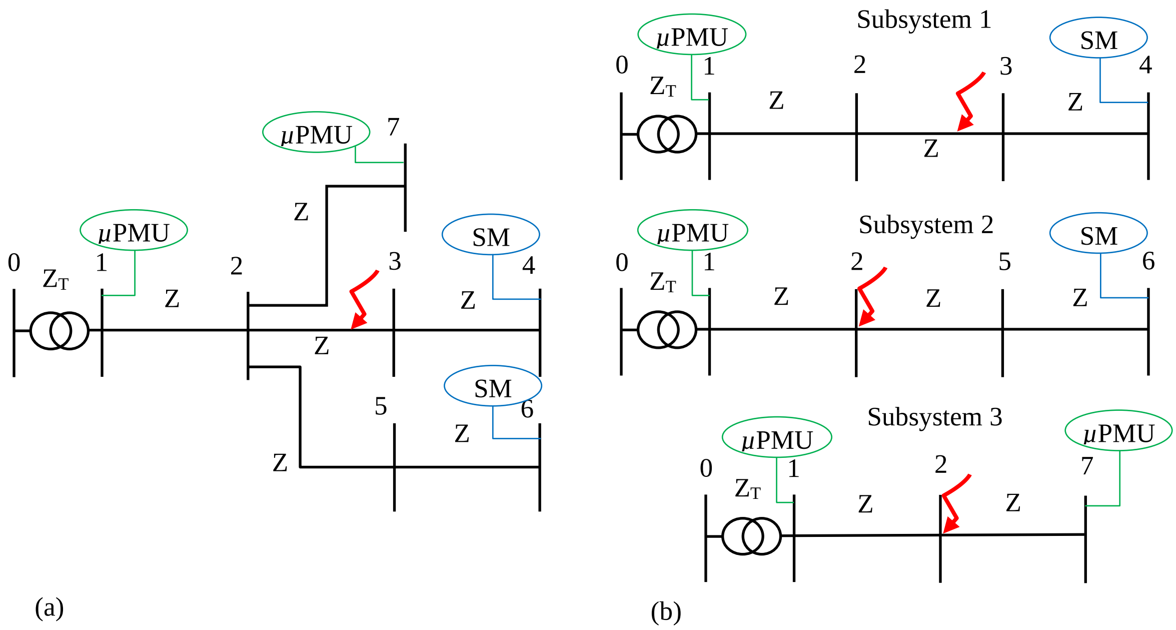

Source: Authors

When a fault occurs at section 2-3, for example, as indicated in Figure 7 (a), all subsystems are affected by the fault as shown in Figure 7 (b). Although the faulted section 2-3 is not present in the subsystems 2 and 3, the fault current is injected into such subsystems by the junction-bus-2, i.e., when a subsystem does not contain the faulted section, the fault current is injected at its junction-bus closest to the fault (such affirmation is valid in a scenario with/without DG). Therefore, since the voltage sags caused at the terminal-bus of each subsystem are associated with the same fault current, any subsystem can be adopted to calculate the fault current.

4.1 FAULT CURRENT CALCULATION

During the fault current calculation, the synchronized pre- and during-fault voltages must be known. Hence, the fault current is calculated from the subsystem equipped with μPMU at its terminal-bus. Arbitrarily, a μPMU is placed at the terminal-bus-7 of the system illustrated in Figure 7. However, as mentioned previously, the fault current could be calculated from any other subsystem with a μPMU at its terminal-bus.

As illustrated in Figure 8, all buses between the substation-bus and the terminal-bus are eliminated for the subsystem equipped with μPMU at its terminal-bus (subsystem 3). From this, the number of measuring devices is equal to the number of buses, which allows the fault current to be calculated from a determined system of equations.

The procedure presented in Figure 8 can also be adopted due to the fault current is significantly higher than the variation of the pre- and during-fault currents of the loads. Furthermore, it must be noted that the series impedance between the substation-bus and the terminal-bus does not change, i.e., the impedance between bus-1 and bus-7 is 2Z for the subsystem 3 in Figure 7 and Figure 8.

Figure 8 – Subsystem 3 only with bus-1 and bus-7, both equipped with μPMU

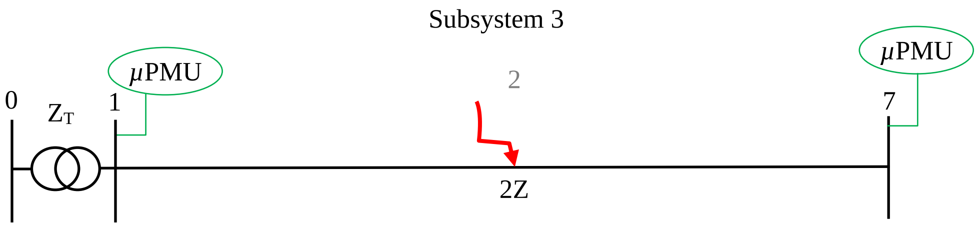

Source: Authors

The voltage sags at buses 1 and 7 are obtained to compose a (6 x 1) voltage sag vector. The voltage sag at each bus is given by (15).

$$\Delta \dot{V}_n^{abc} = \begin{bmatrix} \dot{V}_n^{a,pf} - \dot{V}_n^{a,f} \\ \dot{V}_n^{b,pf} - \dot{V}_n^{b,f} \\ \dot{V}_n^{c,pf} - \dot{V}_n^{c,f} \end{bmatrix}_{3x1} \tag{15}$$

The three-phase impedance matrix of the subsystem 3 is built from the topology shown in Figure 8. By multiplying the inverse of the impedance matrix by the voltage sag vector, a current vector is obtained as described in (16).

$$\begin{bmatrix} -\dot{I}_1^{abc} \\ -\dot{I}_7^{abc} \end{bmatrix}_{6x1} = {}_{inv}\begin{bmatrix} Z_T & Z_T \\ Z_T & Z_T + 2Z \end{bmatrix}_{6x6} \cdot \begin{bmatrix} \Delta \dot{V}_1^{abc} \\ \Delta \dot{V}_7^{abc} \end{bmatrix}_{6x1} \tag{16}$$

The fault current ($\dot{I}_f^{abc}$) is given by the sum of both elements in the current vector, as indicated in (17).

$$\dot{I}_f^{abc} = \dot{I}_1^{abc} + \dot{I}_7^{abc} \tag{17}$$

The subsystems formation procedure shown in Figure 9 is the same with/without DG, i.e., all buses between the substation-bus and terminal-bus are eliminated even if a DG is connected, as illustrated in Figure 9. Such a procedure is adopted due to the low error presented and discussed in item 3.3.

Figure 9 – Fault current calculation procedure under DG presence

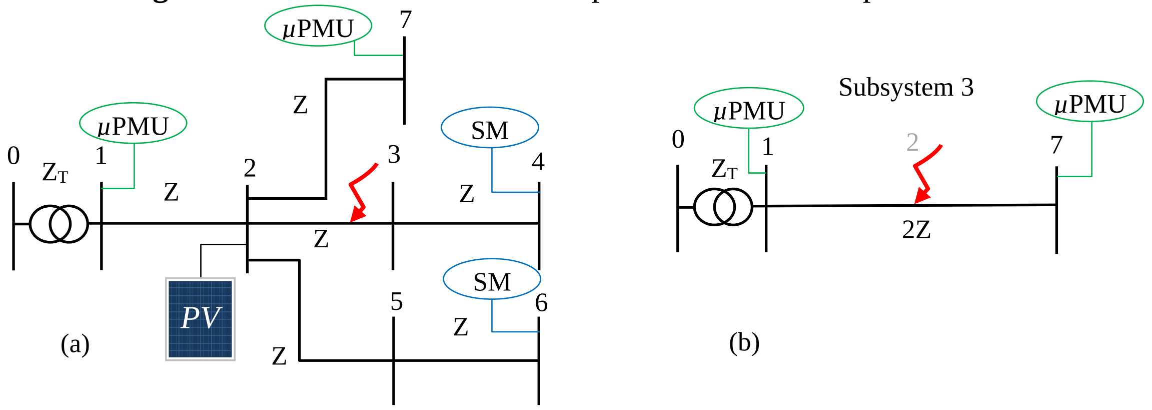

Source: Authors

It is well known that the DG presence changes the pre- and during-fault voltages when compared to a scenario without DG [29]-[30]. Hence, since different voltage sags are applied, the calculated fault current is also changed., i.e., the calculated fault current in (17) is different from the fault current in (19).

$$\begin{bmatrix} -\dot{I}^{abc}_{1,with\_DG} \\ -\dot{I}^{abc}_{7,with\_DG} \end{bmatrix}_{6x1} = inv\begin{bmatrix} Z_T & Z_T \\ Z_T & Z_T+2Z \end{bmatrix}_{6x6} \cdot \begin{bmatrix} \Delta\dot{V}^{abc}_{1,with\_DG} \\ \Delta\dot{V}^{abc}_{7,with\_DG} \end{bmatrix}_{6x1} \tag{18}$$

$$\dot{I}^{abc}_{f,with\_DG} = \dot{I}^{abc}_{1,with\_DG} + \dot{I}^{abc}_{7,with\_DG} \tag{19}$$

4.2 LOCATING THE BUS CLOSEST TO THE FAULT

After calculating the fault current ($\dot{I}^{abc}_f$) from (16) to (19), through the subsystem equipped with μPMUs, the fault location process is performed by investigating the module of the voltage sag at the terminal-bus of all subsystems. For this, measurements of nonsynchronized voltage phasors are required at all terminal-buses, represented by SMs in Figure 7.

Initially, consider only the subsystem 3 of Figure 7 (b). By assuming bus-1 as the faulted bus, a sparse current vector is determined containing the calculated fault current ($\dot{I}^{abc}_f$) at bus-1 position and the other elements set to zero. By multiplying the impedance matrix of the subsystem 3 by the determined sparse current vector, a voltage sag vector is obtained, as (20) where $\Delta\dot{V}^{abc,i}_{m,n}$ is the three-phase voltage sag calculated at terminal-bus-*m* due to a fault current injection at bus-*n*. *i* represents the subsystem under analysis. The same process is performed for all buses of the subsystem 3, as described in (21) and (22). It must be noted in (20), (21), and (22) that the impedance matrix of the subsystem 3 is built by considering all buses, as illustrated in Fig. 7 (b). From (20) to (22), three different voltage sags are calculated for the terminal-bus-7 of the subsystem 3 ($\Delta\dot{V}^{abc,3}_{7,1}$, $\Delta\dot{V}^{abc,3}_{7,2}$, and $\Delta\dot{V}^{abc,3}_{7,7}$).

$$\begin{bmatrix} \Delta\dot{V}^{abc,3}_{1,1} \\ \Delta\dot{V}^{abc,3}_{2,1} \\ \Delta\dot{V}^{abc,3}_{7,1} \end{bmatrix}_{9x1} = \begin{bmatrix} Z_T & Z_T & Z_T \\ Z_T & Z_T+Z & Z_T+Z \\ Z_T & Z_T+Z & Z_T+2Z \end{bmatrix}_{9x9} \cdot \begin{bmatrix} \dot{I}^{abc}_f \\ 0 \\ 0 \end{bmatrix}_{9x1} \tag{20}$$

$$\begin{bmatrix} \Delta\dot{V}_{1,2}^{abc,3} \\ \Delta\dot{V}_{2,2}^{abc,3} \\ \Delta\dot{V}_{7,2}^{abc,3} \end{bmatrix}_{9x1} = \begin{bmatrix} Z_T & Z_T & Z_T \\ Z_T & Z_T+Z & Z_T+Z \\ Z_T & Z_T+Z & Z_T+2Z \end{bmatrix}_{9x9} \cdot \begin{bmatrix} 0 \\ \dot{I}_f^{abc} \\ 0 \end{bmatrix}_{9x1} \tag{21}$$

$$\begin{bmatrix} \Delta\dot{V}_{1,7}^{abc,3} \\ \Delta\dot{V}_{2,7}^{abc,3} \\ \Delta\dot{V}_{7,7}^{abc,3} \end{bmatrix}_{9x1} = \begin{bmatrix} Z_T & Z_T & Z_T \\ Z_T & Z_T+Z & Z_T+Z \\ Z_T & Z_T+Z & Z_T+2Z \end{bmatrix}_{9x9} \cdot \begin{bmatrix} 0 \\ 0 \\ \dot{I}_f^{abc} \end{bmatrix}_{9x1} \tag{22}$$

Assuming the module of the voltage sag measured at the terminal-bus-7 ($|\Delta\dot{V}_7^{abc}|$) as a reference, an error ($Error_{7,n}^{abc,i}$) is attributed for each voltage sag calculated at the terminal-bus-7 ($|\Delta\dot{V}_{7,n}^{abc,i}|$), as described in (23), where $Error_{m,n}^{abc,i}$ is the error attributed for the voltage sag calculated at the terminal-bus-*m* of the subsystem *i* when the fault current is injected at bus-*n*.

$$Error_7^{abc,3} = \begin{bmatrix} Error_{7,1}^{abc,3} \\ Error_{7,2}^{abc,3} \\ Error_{7,7}^{abc,3} \end{bmatrix} = \begin{bmatrix} \left|\Delta\dot{V}_7^{abc}\right| \\ \left|\Delta\dot{V}_7^{abc}\right| \\ \left|\Delta\dot{V}_7^{abc}\right| \end{bmatrix} - \begin{bmatrix} \left|\Delta\dot{V}_{7,1}^{abc,3}\right| \\ \left|\Delta\dot{V}_{7,2}^{abc,3}\right| \\ \left|\Delta\dot{V}_{7,7}^{abc,3}\right| \end{bmatrix} \tag{23}$$

This process, from (20) to (23), is performed for all subsystems. Hence, the error vector results as (24) and (25) for the subsystems 1 and 2, respectively.

$$Error_4^{abc,1} = \begin{bmatrix} Error_{4,1}^{abc,1} \\ Error_{4,2}^{abc,1} \\ Error_{4,3}^{abc,1} \\ Error_{4,4}^{abc,1} \end{bmatrix} = \begin{bmatrix} \left|\Delta\dot{V}_4^{abc}\right| \\ \left|\Delta\dot{V}_4^{abc}\right| \\ \left|\Delta\dot{V}_4^{abc}\right| \\ \left|\Delta\dot{V}_4^{abc}\right| \end{bmatrix} - \begin{bmatrix} \left|\Delta\dot{V}_{4,1}^{abc,1}\right| \\ \left|\Delta\dot{V}_{4,2}^{abc,1}\right| \\ \left|\Delta\dot{V}_{4,3}^{abc,1}\right| \\ \left|\Delta\dot{V}_{4,4}^{abc,1}\right| \end{bmatrix} \tag{24}$$

$$Error_{6}^{abc,2}=\begin{bmatrix} Error_{6,1}^{abc,2} \\ Error_{6,2}^{abc,2} \\ Error_{6,5}^{abc,2} \\ Error_{6,6}^{abc,2} \end{bmatrix}=\begin{bmatrix} \left|\Delta\dot{V}_{6}^{abc}\right| \\ \left|\Delta\dot{V}_{6}^{abc}\right| \\ \left|\Delta\dot{V}_{6}^{abc}\right| \\ \left|\Delta\dot{V}_{6}^{abc}\right| \end{bmatrix}-\begin{bmatrix} \left|\Delta\dot{V}_{6,1}^{abc,2}\right| \\ \left|\Delta\dot{V}_{6,2}^{abc,2}\right| \\ \left|\Delta\dot{V}_{6,5}^{abc,2}\right| \\ \left|\Delta\dot{V}_{6,6}^{abc,2}\right| \end{bmatrix} \quad (25)$$

For each subsystem, different errors are obtained when the fault current is injected at all buses individually. The bus associated with the lowest error of each subsystem is selected and called as “candidate bus”. The candidate bus of each subsystem is used to compose the vector X described in (26). As S subsystems are created, S buses are selected as candidate buses, where x_i is the bus selected as a candidate bus in the subsystem i.

$$X=\begin{bmatrix} x_1 & x_2 & \cdots & x_i & \cdots & x_{S-1} & x_S \end{bmatrix} \quad (26)$$

Considering the fault occurrence at section 2-3, as shown in Figure 7, the lowest error of each subsystem will result for its bus closest to the fault. For explanatory purposes, it is considered that the fault occurs closest to bus-3. Hence, bus-3 is selected as a candidate bus of subsystem 1.

As can be seen in Figure 7 (a), the faulted section 2-3 is not present in the subsystems 2 and 3. As mentioned previously, when a subsystem does not contain the faulted section, the fault current is injected at its junction-bus closest to the fault. Hence, the lowest error will be associated with such a junction-bus. In this case, bus-2 is selected as the candidate bus in both subsystems 2 and 3. Therefore, when a fault occurs at section 2-3, closest to bus-3, the vector X results as (27).

$$X=\begin{bmatrix} 3 & 2 & 2 \end{bmatrix} \quad (27)$$

For a special case, when a fault occurs exactly in the middle of section 2-3, the lowest error of subsystem 1 will be for buses 2 and 3. Under such a condition, any of the buses can be selected as a candidate bus, as both are connected at the faulted section 2-3.

In Table 2, the candidate bus of each subsystem is shown when a fault occurs at all sections of the 7-bus distribution system of Figure 7 (a). For each section, two different fault locations are considered, as illustrated in Figure 10.

Table 2 – Candidate bus of each subsystem for different fault distances

Faulted Section	Fault Distance (%)	Candidate bus of each subsystem		
		x_1	x_2	x_3
1-2	33	1	1	1
	67	2	2	2
2-3	33	2	2	2
	67	3	2	2
3-4	33	3	2	2
	67	4	2	2
2-5	33	2	2	2
	67	2	5	2
5-6	33	2	5	2
	67	2	6	2
2-7	33	2	2	2
	67	2	2	7

Source: Authors

In Figure 10, a section between buses *h* and *k* is illustrated, where l_1 and l_2 represent the distances between the upstream bus (bus-*h*) and the fault locations F_1 and F_2, respectively. Such fault distances are given by the section length percentage.

Figure 10 – Section h-k under two different fault locations

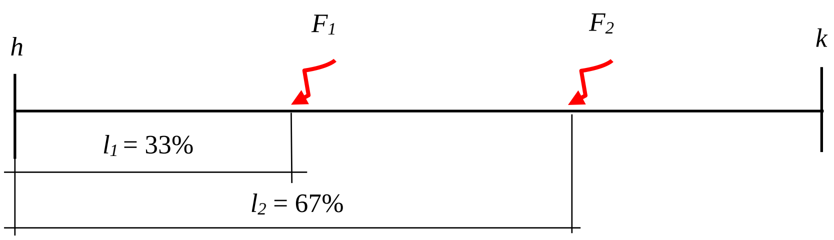

Source: Authors

The vector *X* indicates the candidate bus of each subsystem. However, it is necessary to identify which candidate bus, in (26), is closest to the fault. For this, three additional vectors are created, such as vectors *Y*, *J*, and *W*.

The element y_i of the vector *Y*, in (28), indicates how many subsystems the candidate bus-x_i of the vector *X*, in (26), is present. Bus-3, in (27), is present only in subsystem 1 (one subsystem), and bus-2 in all subsystems 1, 2, and 3 (three subsystems). Therefore, from (27), *Y* results as (29).

$$Y = \begin{bmatrix} y_1 & y_2 & \cdots & y_i & \cdots & y_{S-1} & y_S \end{bmatrix} \quad (28)$$

$$Y = \begin{bmatrix} 1 & 3 & 3 \end{bmatrix} \quad (29)$$

The element j_i of the vector J, in (30), indicates how many times bus-x_i, in (26), has been selected as a candidate bus. Bus-3, in (27), has been selected as a candidate bus only in subsystem 1 (one time), and bus-2 has been selected in subsystems 2 and 3 (two times). Therefore, from (27), the vector J results as (31).

$$J = \begin{bmatrix} j_1 & j_2 & \cdots & j_i & \cdots & j_{S-1} & j_S \end{bmatrix} \tag{30}$$

$$J = \begin{bmatrix} 1 & 2 & 2 \end{bmatrix} \tag{31}$$

Through the vectors Y and J, the weight vector (W) is calculated by (32). Ideally, the bus closest to the fault should be selected as a candidate bus in all subsystems in which it is present. Therefore, the highest weight in (32) indicates which candidate bus in (26) is closest to the fault, where $0 < w_i \leq 1$. For the vectors X, Y and J obtained in (27), (29) and (31), respectively, the vector W results as (33), indicating bus-3 as the bus closest to the fault.

$$W = \begin{bmatrix} \frac{j_1}{y_1} & \frac{j_2}{y_2} & \cdots & \frac{j_i}{y_i} & \cdots & \frac{j_{S-1}}{y_{S-1}} & \frac{j_S}{y_S} \end{bmatrix} \tag{32}$$

$$W = \begin{bmatrix} 1 & \frac{2}{3} & \frac{2}{3} \end{bmatrix} \tag{33}$$

4.3 FAULT LOCATION

After identifying the bus closest to the fault, the faulted section can be located, as well as the faulted point. For this, fictitious buses (dashed buses in Figure 11) are added to all sections connected to bus-3 (bus selected as the bus closest to the fault). Since bus-3 is present only in subsystem 1, such a procedure is applied only for subsystem 1.

Figure 11 – Subsystem 1 with fictitious buses

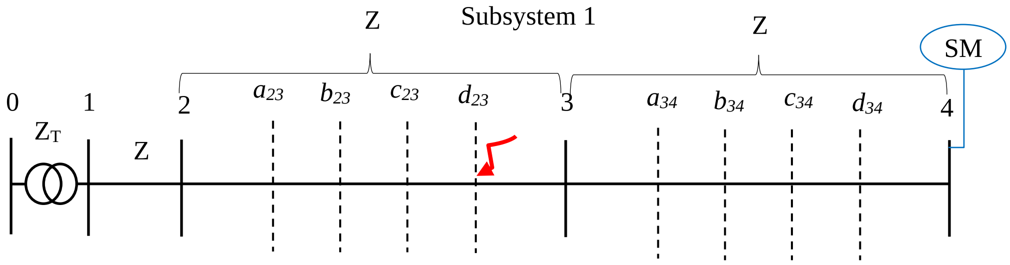

Source: Authors

The impedance matrix of subsystem 1 must be built by considering the topology presented in Figure 11. From this, the process described from (20) to (25) must be repeated only for the subsystem 1. Thus, the fictitious bus presenting the lowest error will indicate the faulted section and the faulted point. Furthermore, the position of the fictitious bus indicates the fault distance.

4.4 FAULT LOCATION FOR SPECIAL CASES

Junction-buses, such as bus-2 in the distribution system in Figure 7 (a), will be present in more than one subsystem. Hence, when a fault occurs close to a junction-bus, it will be present in more than one position in the vector *X*. If the junction-bus is selected as the bus closest to the fault (the highest value in the vector *W*), fictitious buses must be added to all subsystems that contain the junction-bus.

For example, when a fault occurs closest to bus-2 in section 2-3, bus-2 is selected as the bus closest to the fault. In this case, all subsystems must be considered with fictitious buses, as illustrated in Figure 12. Furthermore, as bus-2 was indicated as the bus closest to the fault, the fault may have occurred exactly at bus-2 or at any section connected to bus-2. Therefore, fictitious buses must be added to all sections connected to bus-2.

Figure 12 – Subsystems 1, 2, and 3 with fictitious buses at different sections

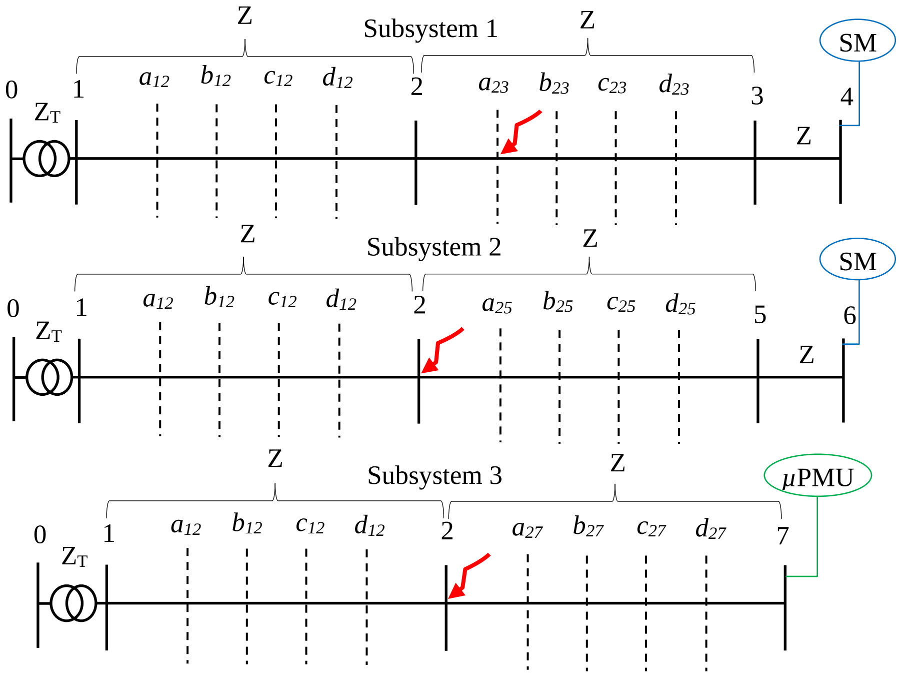

Source: Authors

By repeating the process from (20) to (25) for all subsystems with the topologies in Figure 12 (with fictitious buses), a new vector X is obtained, as (34). As the fault occurred closest to bus-2 in section 2-3, the fictitious bus-a_{23} is selected as a candidate bus in subsystem 1, and bus-2 in subsystems 2 and 3. The new vectors Y, J, and W also result as (29), (31), and (33), respectively. Thus, bus-a_{23} is identified as the fault location.

$$X = [a_{23} \quad 2 \quad 2] \tag{34}$$

Another special case refers to when a fault occurs in a section present in more than one subsystem, for example, when a fault occurs at bus-a_{12} in section 1-2 (Figure 13). Ideally, the faulted bus-a_{12} should be selected as a candidate bus in all subsystems in which it is present. However, as illustrated in Figure 13, adjacent buses such as bus-1 and bus-b_{12} may also be selected as candidate buses. Thus, the new vector X would be composed of bus-1, bus-a_{12}, and bus-b_{12}. Hence, three different fault locations would be identified by the new vector W.

Such a condition may occur due to the proximity between adjacent buses. Based on extensive analyses, it was verified that the pre-fault voltage at the terminal-bus of each subsystem must be investigated. The bus selected in the subsystem with the highest voltage profile is assumed as the faulted point. On the other hand, any of the selected buses could also be adopted arbitrarily, since they will all indicate the same section.

Figure 13 – Subsystems 1, 2, and 3 with fictitious buses in the same section 1-2

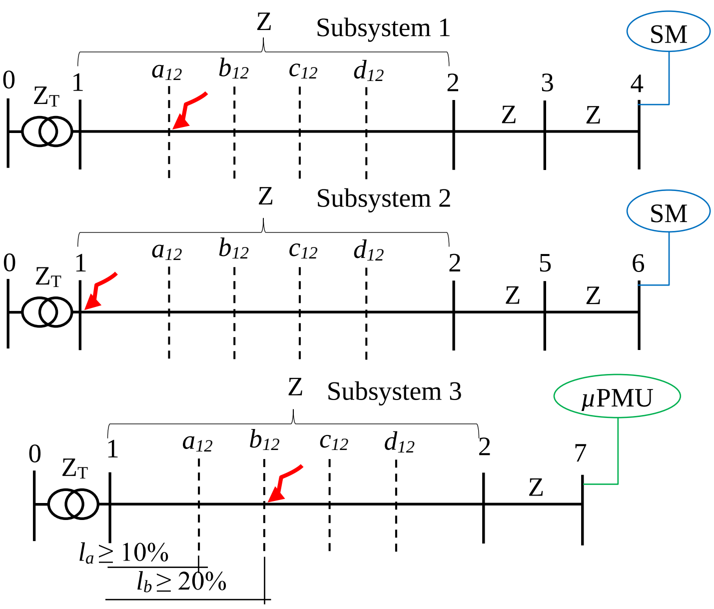

Source: Authors

To decrease the possibility of selecting different buses in the same section, fictitious buses could be added so that a distance of at least 10% is obtained between all adjacent buses, as shown in subsystem 3 of Figure 13. The proposed method is described in detail in Figure 14.

Figure 14 – Flowchart of the proposed method for fault location

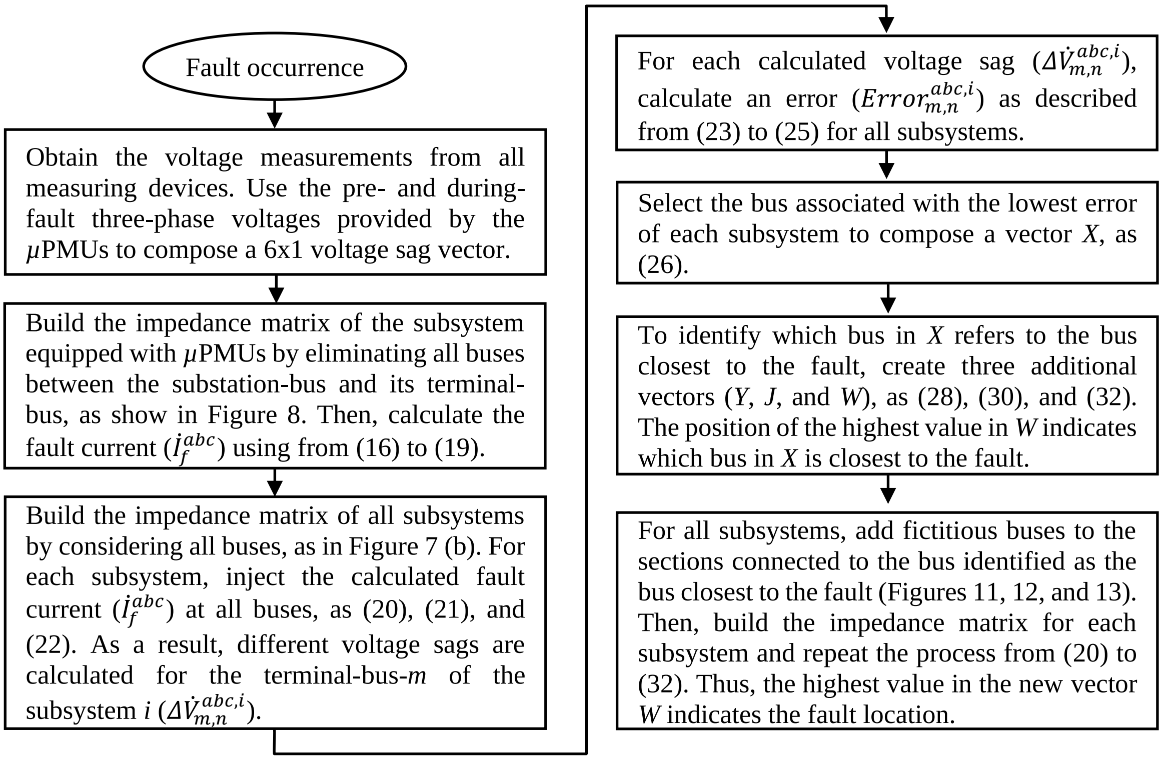

Source: Authors

4.5 ANALYSES OF THE DG EFFECTS ON THE PROPOSED METHOD

In order to verified the DG effects on the proposed method performance, the 8-bus distribution system is considered under four different scenarios, as indicated in Figure 15. For all scenarios, a LG fault is caused at bus-6 with a fault resistance of 10 ohms. By employing the proposed method, the fault location is estimated for each scenario, where the fault location results are described in Table 3. For the scenarios with DG (scenarios 2, 3, and 4), all DGs are inserted as synchronous DG (SDG) with 200 kVA.

In scenario 1, the proposed method indicated that a fault occurred exactly at bus-6 (0% of section 6-7). When a 200 kVA SDG1 is placed at bus-3 (scenario 2), the method presented an error of 10%. On the other hand, the method did not present any error when an additional 200kVA SDG2 is also placed at bus-8 (scenario 3). Finally, an error of 5% is obtained by installing the 200 kVA SDG2 at bus-7 (scenario 4).

Figure 15 – The 8-bus distribution system under different scenarios

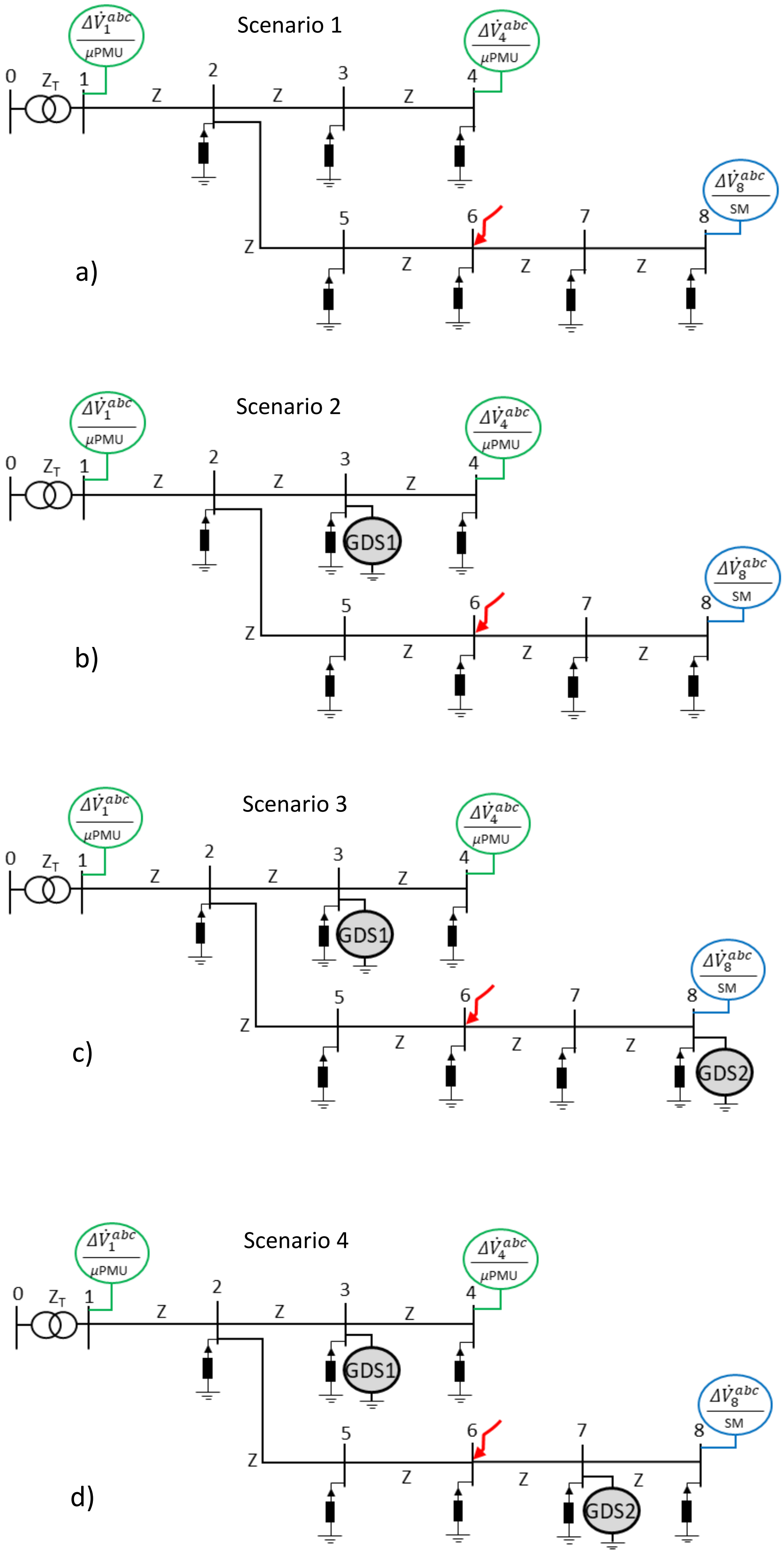

Source: Authors

Table 3 – Fault location results when a fault occurs at bus-6 of the 8-bus system

Scenarios	Buses with Synchronous DG (SDG)	Actual fault location	Relative fault location estimated by the proposed method
1	-	0% of section 6-7	0% of section 6-7
2	bus-3	0% of section 6-7	10% of section 6-7
3	bus-3 and bus-8	0% of section 6-7	0% of section 6-7
4	bus-3 and bus-7	0% of section 6-7	5% of section 6-7

Source: Authors

As can be seen in Table 3, the worst fault location result was obtained for the scenario 2, when only one SDG1 is placed in the 8-bus system. Furthermore, it is noted that the method performance can be improved when two SDGs are placed in the system (scenarios 3 and 4).

As discussed previously, in item 4.1, the voltage sags caused during the fault occurrence are also impacted by the DG presence. Therefore, DGs effects described in Table 3 can be explained by investigating the voltage sags caused at the terminal-buses during a fault. For illustrative purposes and to better highlight the DG effects, the faulted subsystem in the scenario 3 is illustrated in Figure 16.

Figure 16 – Faulted subsystem of scenario 3

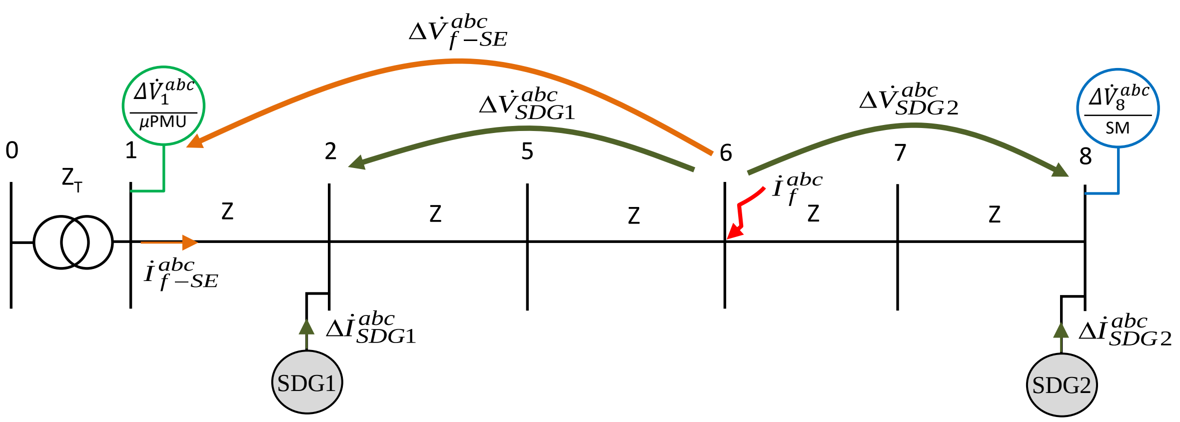

Source: Authors

The 8-bus system has two terminal-buses (bus-4 and bus-8) and, hence, two subsystems. For the analyses, the fault is also considered at the subsystem formed by buses 1 and 8, at bus-6 specifically. For the scenario 3, the fault is supplied by all sources (substation source, SDG1, and SDG2). As can be seen in Figure 15 c), the SDG 1 is not present in the faulted subsystem. In this case, the fault current contribution of the SDG1 is injected at the faulted subsystem by the junction-bus-2. Therefore, as illustrated in Figure 16, when analyzing the faulted subsystem, the SDG1 can be considered at the junction-bus-2 regardless of where it is connected in the subsystem formed by buses 1 and 4.

From Figure 16, the voltage sag at terminal-bus 8 can be calculated according to (35), where $\Delta\dot{V}_8^{abc}$is the voltage sag at bus-8 caused by the fault current $\dot{I}_f^{abc}$, $\Delta\dot{V}_{f-SE}^{abc}$ is the voltage sag caused by the substation fault current contribution $\dot{I}_{f-SE}^{abc}$, $\Delta\dot{V}_{SDG1}^{abc}$ is the voltage sag caused by the SDG1 fault current contribution $\Delta\dot{I}_{SDG1}^{abc}$, and the $\Delta\dot{V}_{SDG2}^{abc}$ is the voltage sag caused by the SDG2 fault current contribution $\Delta\dot{I}_{SDG2}^{abc}$.

$$\Delta\dot{V}_8^{abc} = \Delta\dot{V}_{f-SE}^{abc} + \Delta\dot{V}_{SDG1}^{abc} - \Delta\dot{V}_{SDG2}^{abc} \tag{35}$$

Since both SDG1 and SDG2 have the same power of 200 kVA, as well as the same distance from the faulted point, (36) is valid for the small 8-bus system under analysis.

$$\Delta\dot{V}_{SDG1}^{abc} = \Delta\dot{V}_{SDG2}^{abc} \tag{36}$$

By substituting (36) in (35), (37) is obtained. That is, in scenario 3, the voltage sag at bus-8 is caused only by the substation fault current contribution, since the SDGs fault current contributions are canceled. Therefore, the same results are obtained for the scenarios 1 and 3.

$$\Delta\dot{V}_8^{abc} = \Delta\dot{V}_{f-SE}^{abc} \tag{37}$$

5. VALIDATION OF THE PROPOSED METHOD

DIgSILENT software is utilized to model the distribution network. The performance of the proposed method is validated on the IEEE 33-bus, 12.66 kV distribution network presented in Figure 17, where the system data are available in [31]. A 10 MVA three-phase transformer is used in the substation with resistance and reactance of 1% and 7%, respectively. The loads were modeled as constant-power loads.

Figure 17 – Diagram of the 33-bus, 12.66 kV distribution system

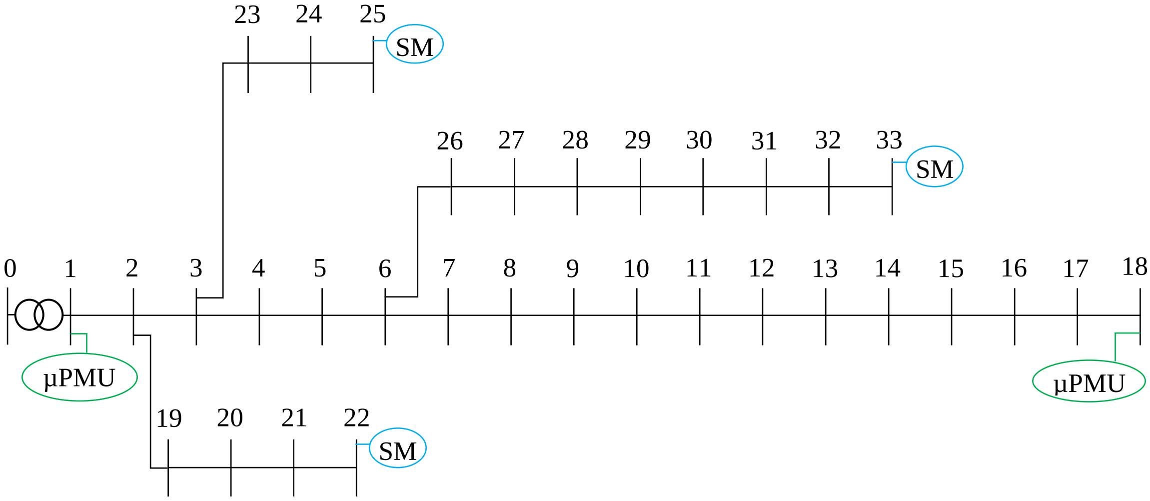

Source: Authors

As shown in Figure 17, two μPMUs and three SMs are required for the 33-bus system, totaling 5 measuring devices. A μPMU is placed arbitrarily at bus-18. The method is validated under several pre- and during fault scenarios. However, before presenting the proposed method performance for different conditions, the fault current calculation procedure is discussed through numerical results. Moreover, in order to illustrate the subsystem formation procedure for a larger distribution network, the proposed subsystems are illustrated in Figure 18 for the 33-bus system.

Figure 18 – (a) Proposed subsystems used to inject the calculated fault current; (b) Proposed subsystems used to calculate the fault current

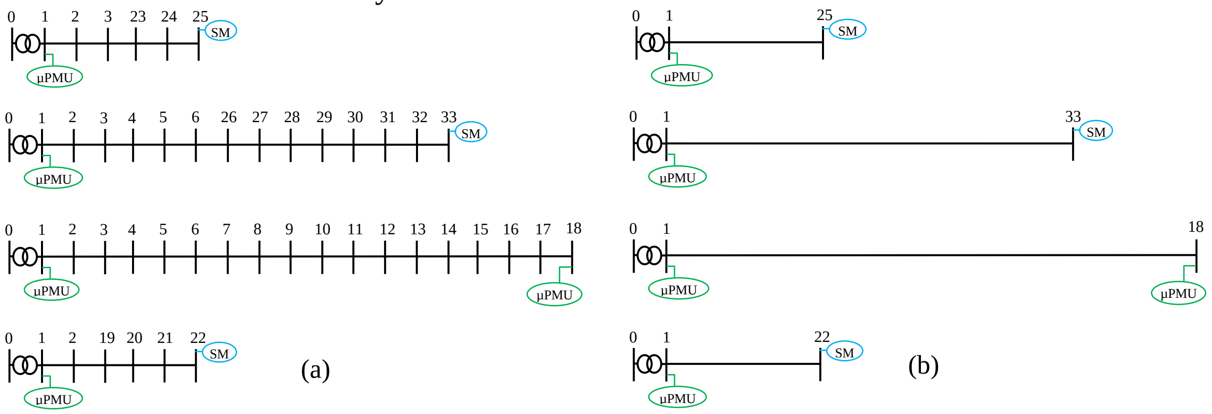

Source: Authors

5.1 NUMERICAL PROCEDURE FOR THE FAULT CURRENT CALCULATION

As discussed, the proposed method assumes that the loads current variation is zero during the fault current calculation, the same fault current calculation procedure is adopted for both scenarios with/without DG, and it is stated that any subsystem can be adopted to calculate the fault current. Thus, numerical results are presented showing such statements.

In Table 4, synchronized pre- and during-fault phase voltages obtained at bus-1 and bus-18 are specified when the 33-bus system does not contain DG and when the 33-bus system contains a 500 kW PV at bus-12. In DIgSILENT, for both scenarios, LG fault is simulated at 50% of section 5-6 with a fault resistance of 5 ohms. The data in Table 4 refer to phase A, where the fault is simulated.

Table 4 – Voltage profile at buses 1 and 18 of the 33-bus system

DG	Bus	Pre-fault phase voltage	During-fault phase voltage
No	1	$7.197\angle -0.97°$ (kV)	$6.801\angle -9.29°$ (kV)
	18	$6.815\angle -1.15°$ (kV)	$4.727\angle -18.49°$ (kV)
Yes	1	$7.202\angle -0.76°$ (kV)	$6.808\angle -9.16°$ (kV)
	18	$6.960\angle -0.18°$ (kV)	$4.829\angle -17.22°$ (kV)

Source: Authors

In Table 4, the fault current values, calculated by the proposed method, are specified. For this, the impedance matrix of the subsystem with the terminal bus-18 (topology of Figure 18 (b)) is used as well as the voltage values in Table 4.

Table 5 – Fault current value when an LG fault occurs at section 5-6 of the 33-bus system

DG	DIgSILENT fault current	Calculated fault Current
No	975 A	963 A
Yes	981 A	971 A

Source: Authors

In Table 4, it can be noted that the DG presence changes the pre- and during-fault voltages at all buses. Hence, different fault currents are obtained when different voltage sags are applied. For comparative purposes, the fault current recorded in DIgSILENT is also shown in Table 5.

As mentioned, the LG fault was simulated at 50% of section 5-6. The method estimated the fault at 44% of section 5-6 for both scenarios with and without the PV system, showing very good results for the fault current calculation and location procedures.

As presented in item 4.1, after multiplying the impedance matrix by the synchronized voltage sag vector for each subsystem, two values are obtained (equations (16) and (18)), and the fault current is obtained by summing both values (equations (17) and (19)). Therefore, in Table 6, the fault current calculation results are shown when the fault current is calculated from all subsystems, i.e., by considering all terminal-buses equipped with μPMU. The fault is calculated for the scenario in which the 500 kW PV unit is installed at bus-12.

Table 6 – Fault current value calculated by each subsystem

Subsystem (1-k)	Resulting value at substation-bus (I_1)	Resulting value at terminal-bus (I_k)	$I_{cc} = I_1 + I_k$	$\lvert I_{cc}\rvert$
1-22	(9.067 - j2.818) 10^2 A	(0.182 - j0.149) 10^2 A	(9.249 - j2.967) 10^2 A	971 A
1-25	(7.666 - j2.153) 10^2 A	(1.584 - j0.814) 10^2 A	(9.249 - j2.967) 10^2 A	971 A
1-33	(7.261 - j1.993) 10^2 A	(1.988 - j0.974) 10^2 A	(9.249 - j2.967) 10^2 A	971 A
1-18	(8.061 - j2.364) 10^2 A	(1.188 - j0.603) 10^2 A	(9.249 - j2.967) 10^2 A	971 A

Source: Authors

After presenting numerical analyses for the fault current calculation procedure, the method performance is investigated under several pre- and during fault scenarios. For each scenario, two faults were simulated at all sections (at 33% and 67% of each section) as illustrated in Figure 10, resulting in 64 fault cases. During the faulted point location, 8 fictitious buses were added to the sections under analysis, resulting in a distance of 11.11% between all adjacent buses.

5.2 METHOD SENSITIVITY TO THE FAULT RESISTANCE

In Table 7, single-line to ground fault (LG) is addressed. For all cases, the same results are obtained when the fault resistance ranges from 1 to 100 ohms (it is was used 1, 50, and 100 Ω). The proposed method is insensitive to the fault resistance due to its effect is already included in the measured during-fault voltages. In Tables 6, the actual and calculated fault distance at each section refer to the section length percentage.

Table 7 – Fault simulation results under different fault resistances

Faulted Section	Fault Type	Fault Resistance (Ω)	Fault distance simulated at each section (%)	Calculated Faulted Section	Calculated fault distance at each section (%)
1-2	LG	1, 50, 100	33 / 67	1-2 / 1-2	22 / 56
2-3	LG	1, 50, 100	33 / 67	2-3 / 2-3	22 / 67
3-4	LG	1, 50, 100	33 / 67	3-4 / 3-4	22 / 56
4-5	LG	1, 50, 100	33 / 67	4-5 / 4-5	11 / 56
5-6	LG	1, 50, 100	33 / 67	5-6 / 5-6	22 / 56
6-7	LG	1, 50, 100	33 / 67	6-7 / 6-7	22/ 56
7-8	LG	1, 50, 100	33 / 67	7-8 / 7-8	22 / 56
8-9	LG	1, 50, 100	33 / 67	8-9 / 8-9	33 / 67
9-10	LG	1, 50, 100	33 / 67	9-10 / 9-10	33 / 67
10-11	LG	1, 50, 100	33 / 67	10-11 / 10-11	11 / 44
11-12	LG	1, 50, 100	33 / 67	11-12 / 11-12	22 / 56
12-13	LG	1, 50, 100	33 / 67	12-13 / 12-13	33 / 67
13-14	LG	1, 50, 100	33 / 67	13-14 / 13-14	33 / 67
14-15	LG	1, 50, 100	33 / 67	14-15 / 14-15	33 / 67
15-16	LG	1, 50, 100	33 / 67	15-16 / 15-16	33 / 78
16-17	LG	1, 50, 100	33 / 67	16-17 / 16-17	33 / 67
17-18	LG	1, 50, 100	33 / 67	17-18 / 17-18	44 / 78
2-19	LG	1, 50, 100	33 / 67	2-19 / 2-19	33 / 67
19-20	LG	1, 50, 100	33 / 67	19-20 / 19-20	33 / 67
20-21	LG	1, 50, 100	33 / 67	20-21 / 20-21	33 / 67
21-22	LG	1, 50, 100	33 / 67	21-22 / 21-22	33 / 67
3-23	LG	1, 50, 100	33 / 67	3-23 / 3-23	33 / 67
23-24	LG	1, 50, 100	33 / 67	23-24 / 23-24	33 / 67
24-25	LG	1, 50, 100	33 / 67	24-25 / 24-25	33 / 67
6-26	LG	1, 50, 100	33 / 67	6-26 / 6-26	0 / 33
26-27	LG	1, 50, 100	33 / 67	26-27 / 26-27	11 / 44
27-28	LG	1, 50, 100	33 / 67	27-28 / 27-28	33 / 67
28-29	LG	1, 50, 100	33 / 67	28-29 / 28-29	22 / 67
29-30	LG	1, 50, 100	33 / 67	29-30 / 29-30	22 / 56
30-31	LG	1, 50, 100	33 / 67	30-31 / 30-31	33 / 67
31-32	LG	1, 50, 100	33 / 67	31-32 / 31-32	33 / 67
32-33	LG	1, 50, 100	33 / 67	32-33 / 32-33	33 / 78

Source: Authors

As can be seen in Table 7, the faulted section was indicated correctly in 63 cases (98.44% of the cases). Only in a case, when a fault occurs at 33% of section 6-26, bus-6 was indicated incorrectly as the faulted point. In this case, since bus-6 is connected to three different sections, it is not possible to identify the actual faulted section. However, all three sections refer to adjacent sections. Thus, it is assumed that the algorithm indicates an adjacent section of the actual faulted section.

Besides indicating the faulted section accurately, the proposed method indicates in which half of the section the fault is located. When the indicated distance is ≤ 44%, it means that the fault occurred in the first half (between 1% and 50% of the section length). When the indicated distance is ≥ 56%, it means that the fault occurred in the second half (between 50% and 100% of the section length). Therefore, from 63 sections indicated correctly, 60 were indicated in the correct half (95.24%). Finally, from 60 half sections indicated accurately, 36 refer to the exact point of the fault (60%). From these analyses, Table 7 can be summarized in Table 8.

Table 8 – Method sensitivity to the fault resistances

Fault type	Fault resistance	Correct section	Adjacent Section	Correct half	Exact point
LG	1 Ω	63	1	60	36
LG	50 Ω	63	1	60	36
LG	100 Ω	63	1	60	36

Source: Authors

5.3 METHOD SENSITIVITY UNDER UNBALANCED SYSTEM CONDITION

In order to investigate the method sensitivity under an unbalanced system condition, the loads present in phase A and phase C were decreased and increased by 20%, respectively. The loads present in phase B were not changed. The results described in Table 9 show the robustness of the method under an unbalanced system condition for all fault types.

Table 9 – Simulation results under unbalanced system condition

Fault type	Fault resistance	Correct section	Adjacent Section	Correct half	Exact point
LLL	1, 50, 100 Ω	62	2	57	30
LL	1, 50, 100 Ω	62	2	55	33
LLG	1, 50, 100 Ω	62	2	58	30
AG	1, 50, 100 Ω	63	1	60	35
BG	1, 50, 100 Ω	63	1	59	32
CG	1, 50, 100 Ω	63	1	60	36

Source: Authors

5.4 METHOD SENSITIVITY UNDER DIFFERENT LOADING CONDITION

In Table 10, the simulation results are shown when all loads are increased and decreased by 30%. The method sensitivity can be verified by analyzing the exact point of the fault. Even under high loading conditions, the correct section was indicated accurately. In the worst case, 95.31% of the sections were indicate correctly, with 93.44% representing the correct half.

Table 10 – Simulation results for different loading scenarios

Total Load	Fault type	Fault resistance	Correct section	Adjacent Section	Correct half	Exact point
70%	LG	1, 50, 100 Ω	62	2	59	41
100%	LG	1, 50, 100 Ω	63	1	60	36
130%	LG	1, 50, 100 Ω	61	3	57	28

Source: Authors

5.5 METHOD SENSITIVITY BY CONSIDERING LINE PARAMETER ERRORS

Line parameters in distribution networks may be obtained with errors. From this, the method sensitivity is investigated by attributing errors of +5% and -5% to the impedance of some sections, as indicated in Table 11.

Table 11 – Errors attributed arbitrarily to the impedance of some sections

Section	Impedance change percentage
1-2	+5%
7-8	-5%
10-11	+5%
11-12	-5%
17-18	+5%
20-21	+5%
24-25	-5%
27-28	+5%
30-31	-5%

Source: Authors

Assuming the errors in Table 11, the simulation results are described in Table 12. By comparing Tables 8 and 12, for LG fault type, it is verified that when the impedance matrix of each subsystem is constructed based on incorrect data, the exact fault location (exact point) is affected. However, the correct section and correct half are indicated accurately with 96.87% and 87%, respectively.

Table 12 – Simulation results under line parameter errors

Fault type	Fault resistance	Correct section	Adjacent Section	Correct half	Exact point
LLL	1, 50, 100 Ω	62	2	54	16
LL	1, 50, 100 Ω	62	2	54	16
LLG	1, 50, 100 Ω	62	2	56	22
LG	1, 50, 100 Ω	63	1	58	24

Source: Authors

5.6 METHOD SENSITIVITY UNDER VOLTAGE MEASUREMENT ERRORS

According to [10], [16], and [21], the error of voltage measuring devices ranges from 0.1 - 0.5%. In fact, according to the datasheet provided by the power standards lab (PSL), ultra-accurate phasor measurements of +-0.01% can be obtained from μPMUs. However, to further explore the accuracy of the proposed method, an error of +0.5 and -0.5% was assumed for all measuring devices, as presented in Table 13.

Table 13 – Errors attributed arbitrarily to the measuring devices

Measurement devices	Voltage errors
At bus-1 (μPMU)	+0.5%
At bus-18 (μPMU)	-0.5%
At bus-22 (SM)	+0.5%
At bus-25 (SM)	-0.5%
At bus-33 (SM)	+0.5%

Source: Authors

In Table 14, simulation results are shown by considering the errors described in Table 13. Although the voltage measurement errors also affect the exact point location, 92.19% of the sections were indicated correctly. From 59 correct sections, 50 (worst case) was indicated in the correct half, representing 84.75%.

Table 14 – Simulation results under voltage measurement errors condition

Fault type	Fault resistance	Correct section	Adjacent Section	Correct half	Exact point
LLL	1, 50, 100 Ω	59	5	52	19
LL	1, 50, 100 Ω	59	5	50	25
LLG	1, 50, 100 Ω	59	5	52	17
LG	1, 50, 100 Ω	59	5	52	15

Source: Authors

It is important to note that the results in Table 14 were obtained when the μPMUs at bus-1 and bus-18 have an error of +0.5% and -0.5%, respectively. In this case, the fault current is calculated under an error of 1%. In Table 15, the simulation results are presented, only for LLL fault, when an error of +0.5% is also adopted for the μPMU placed at bus-18. In this condition, the method is less affected.

Table 15 – Simulation results under voltage measurement errors condition

Fault type	Fault resistance	Correct section	Adjacent Section	Correct half	Exact point
LLL	1, 50, 100 Ω	62	2	57	20

Source: Authors

5.7 METHOD SENSITIVITY UNDER DG PRESENCE

As illustrated in Figure 19, six DGs are added arbitrarily to the IEEE 33-bus, 12.66 kV distribution system. The capacity of each DG, location, and type are indicated in Table 16. The quantity of DGs, as well as their capacity, were adopted based on the method proposed in [22]. The total capacity of all DG units represents 59% of the total loads on the system.

Figure 19 – Diagram of the 33-bus, 12.66 kV distribution system with DGs

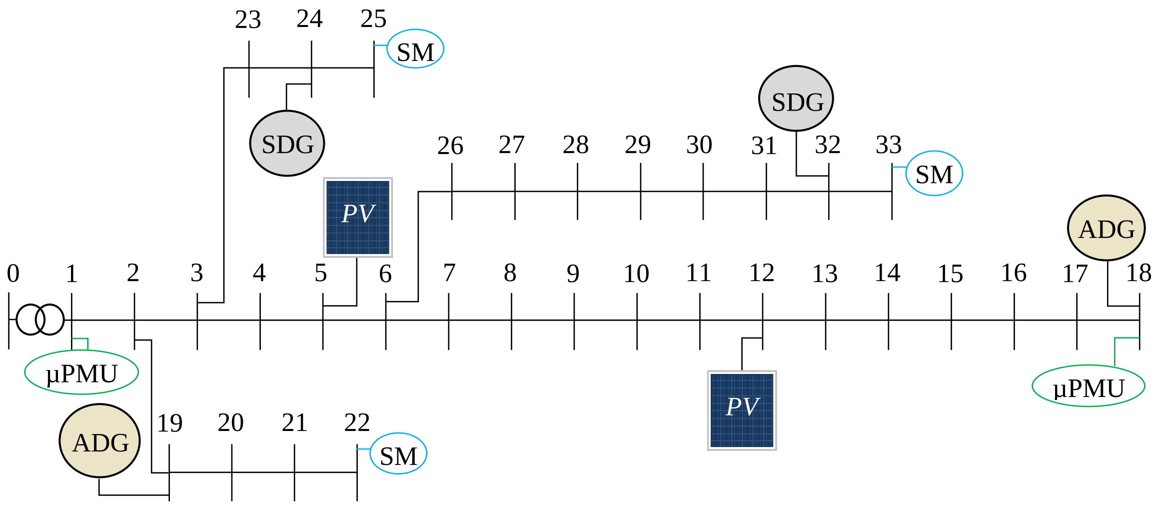

Source: Authors

Table 16 – Data of the distributed generators installed in the 33-bus system (configuration 1)

Bus	**DG type**	**Capacity**
5	Photovoltaic (PV)	250 kW
12	Photovoltaic (PV)	550 kW
18	Asynchronous (ADG)	100 kVA
19	Asynchronous (ADG)	300 kVA
24	Synchronous (SDG)	500 kVA
32	Synchronous (SDG)	100 kVA

Source: Authors

The method performance with DGs is specified in Table 17. Although the method performance is affected under DG presence, very good results are still achieved. In the worst case, 90.63% of the sections were indicated correctly. From 58 correct sections, 45 were indicated in the correct half.

LG fault is the most common fault in distribution networks [2]. As can be seen in Table 17, the method is further robust for this fault type. Correct sections were indicated accurately in 98.44% of the fault cases. From 63 correct sections, 85.71% were indicated in the correct half.

Table 17 – Simulation results under DG presence allocated according to Table 16

Fault type	**Fault resistance**	**Correct section**	**Adjacent Section**	**Correct half**	**Exact point**
LLL	1, 50, 100 Ω	59	5	45	15
LL	1, 50, 100 Ω	58	6	45	15
LLG	1, 50, 100 Ω	62	2	53	11
LG	1, 50, 100 Ω	63	1	54	22

Source: Authors

In Table 18, the method performance, for LG fault, is presented when the DGs described in Table 16 are placed at different buses, as indicated in Table 19.

Table 18 – Simulation results under DG presence allocated according to Table 19

Fault type	**Fault resistance**	**Correct section**	**Adjacent Section**	**Correct half**	**Exact point**
LG	1, 50, 100 Ω	60	4	48	19

Source: Authors

Table 19 – Data of the distributed generators installed in the 33-bus system (configuration 2)

Bus	DG type	Capacity
29	Photovoltaic (PV)	250 kW
23	Photovoltaic (PV)	550 kW
33	Asynchronous (ADG)	100 kVA
16	Asynchronous (ADG)	300 kVA
4	Synchronous (SDG)	500 kVA
22	Synchronous (SDG)	100 kVA

Source: Authors

In Table 18, 4 adjacent sections are indicated incorrectly when the DG configuration is changed according to Table 19. Table 20 is presented indicating the cases in which such adjacent sections were pointed out as the faulted section. In fact, only in a case, an adjacent section was indicated (at a point very close to the faulted bus). In other cases, one of the boundaries of the faulted section (its upstream or downstream bus) was indicated, resulting in a relative error of 33%. Therefore, from these analyses, the method robustness can be verified.

Table 20 – Cases in which adjacent sections were indicated incorrectly in the 33-bus system

Faulted Section	Fault Type	Fault Resistance	Fault distance simulated at each section (%)	Calculated Faulted Section	Calculated fault distance at each section (%)
10-11	LG	1, 50, 100 Ω	33	10-11	0
15-16	LG	1, 50, 100 Ω	67	15-16	100
6-26	LG	1, 50, 100 Ω	33	6-26	0
31-32	LG	1, 50, 100 Ω	67	32-33	11

Source: Authors

In order to further investigate the method sensitivity under DG presence, a synchronous DG is placed at bus-25 of the 33-bus system. Under such a scenario, LG faults are simulated at 50% of section 12-13, varying the DG power from 0 to 500 kVA. As a result, the graph in Figure 20 is obtained by relating the method error with the DG power, where it is verified an error of 10% for the worst case when the DG power is 500 kVA. In this case, the method estimates the fault at 60% of section 5-6, representing a very attractive fault location result.

Figure 20 – Graph of Error (%) versus SDG (kVA) for LG fault at 50% of section 12-13 when DG is placed at bus-25

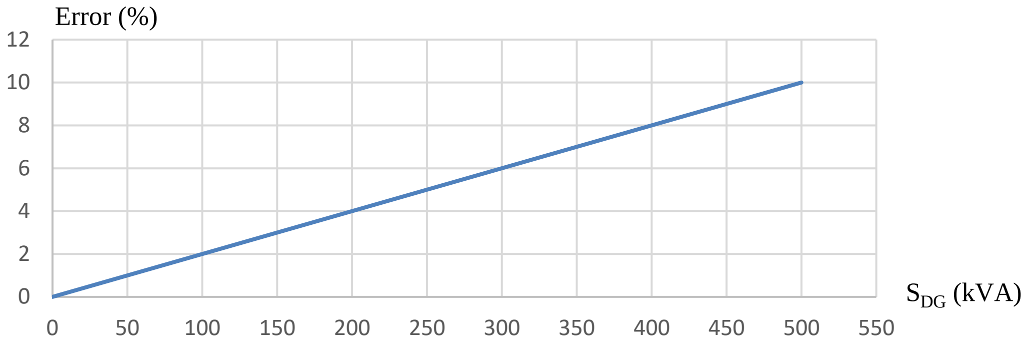

Source: Authors

In Figure 21, the method sensitivity is presented when a synchronous DG is placed at bus-23 of the 33-bus system. Under such a scenario, LG faults are also simulated at 50% of section 12-13, varying the DG power from 0 to 500 kVA. As a result, the graph in Figure 21 is obtained, where it is verified an error of 4% for the worst case when the DG power is 500 kVA. In this case, the method estimates the fault at 54% of section 5-6.

Figure 21 – Graph of Error (%) versus S_{DG} (kVA) for LG fault at 50% of section 12-13 when DG is placed at bus-23

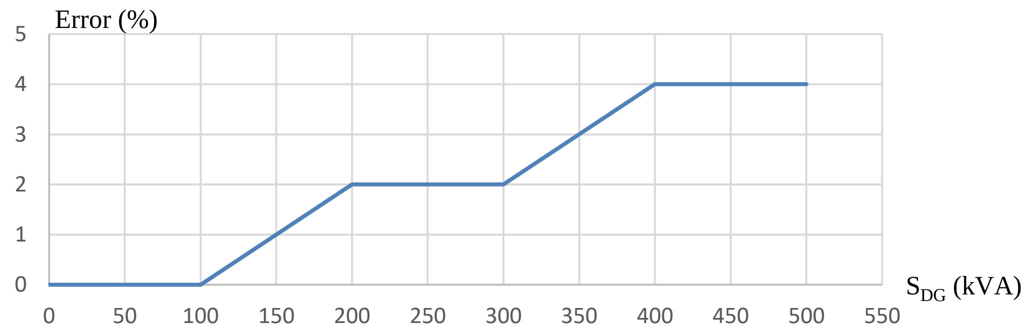

Source: Authors

It is well known that the fault current contribution of DGs is higher when a fault occurs close to the DG coupling point. On the other hand, it can be noted, by comparing Figures 18 and 19, that the closer the DG is to the fault, the lower the error presented by the proposed method.

5.8 METHOD SENSITIVITY TO THE LOAD MODEL VARIATION

In this analysis, the method performance is investigated by modeling all loads as constant power (P), constant current (I) and constant impedance (Z). The simulation results are presented in Table 21, where, for the worst case, 96.87% of the sections were indicated correctly, with 85.48% representing the correct half.

Table 21 – Method sensitivity to the loads model

Loads Model	Fault type	Fault resistance	Correct section	Adjacent Section	Correct half	Exact point
Z	LG	1, 50, 100 Ω	63	1	57	29
I	LG	1, 50, 100 Ω	62	2	55	29
P	LG	1, 50, 100 Ω	62	2	53	29

Source: Authors

5.9 SIMULATION RESULTS FOR THE IEEE 69-BUS DISTRIBUTION SYSTEM

In order to further investigate the robustness of the proposed method, simulations are also performed on the IEEE 69-bus, 12.66 kV distribution system shown in Figure 22 [32].

Figure 22 – Diagram of the 69-bus, 12.66 kV distribution system

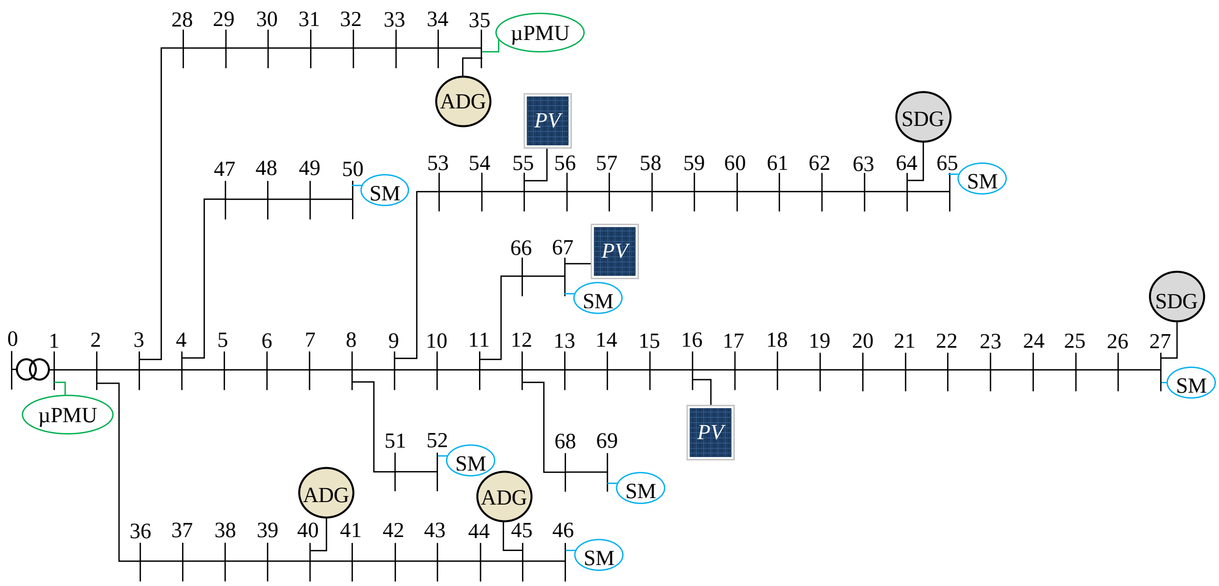

Source: Authors

Arbitrarily, eight DGs, described in Table 22, are installed. Two faults are also considered for each section of the 69-bus system (Figure 10), resulting in 136 cases for each scenario. For these analyses, the total capacity of all DG units represents 64% of the total loads on the system.

Table 22 – Data of the distributed generators installed in the 69-bus system

Bus	DG type	Capacity
16	Photovoltaic (PV)	300 kW
55	Photovoltaic (PV)	250 kW
67	Photovoltaic (PV)	150 kW
35	Asynchronous (ADG)	50 kVA
40	Asynchronous (ADG)	100 kVA
45	Asynchronous (ADG)	150 kVA
27	Synchronous (SDG)	200 kVA
64	Synchronous (SDG)	300 kVA

Source: Authors

In Table 23, very good location results are also verified for the 69-bus system with/without DG. The percentage of correct sections ranges from 80% to 92.65%. From Tables 17 and 23, similar results can be verified for different systems. For both systems, only correct and adjacent sections are identified, and the location results are more robust for LG faults.

Table 23 – Simulation results for the 69-bus system

DG	Fault type	Fault resistance	Correct section	Adjacent Section	Correct half	Exact point
No	LG	1, 50, 100 Ω	126	10	119	78
	LLL		125	11	113	64
Yes	LG	1, 50, 100 Ω	120	16	106	67
	LLL		108	28	90	49

Source: Authors

The simulation results in Table 23 show that the number of adjacent sections increases in a scenario with DG. However, indicating adjacent sections still represents a very attractive location result. Thus, the cases in which such adjacent sections have been pinpointed, under DG presence, are described in the Table 24 for LG fault. In Table 24, it can be noted that in most of the cases in which an adjacent section was indicated, in fact, its upstream bus or downstream bus was pinpointed.

Table 24 – Cases in which adjacent sections were indicated incorrectly in the 69-bus system

Faulted Section	Fault Type	Fault Resistance	Fault distance simulated at each section (%)	Calculated Faulted Section	Calculated fault distance at each section (%)
8-9	LG	1, 50, 100 Ω	33	8-9	0
17-18	LG	1, 50, 100 Ω	33	17-18	0
17-18	LG	1, 50, 100 Ω	67	17-18	0
21-22	LG	1, 50, 100 Ω	33	22-23	33
21-22	LG	1, 50, 100 Ω	67	22-23	33
22-23	LG	1, 50, 100 Ω	67	22-23	100
25-26	LG	1, 50, 100 Ω	67	25-26	100
3-28	LG	1, 50, 100 Ω	33	2-3	0
2-36	LG	1, 50, 100 Ω	33	1-2	0
39-40	LG	1, 50, 100 Ω	33	39-40	100
39-40	LG	1, 50, 100 Ω	67	39-40	100
42-43	LG	1, 50, 100 Ω	67	42-43	100
43-44	LG	1, 50, 100 Ω	33	43-44	0
43-44	LG	1, 50, 100 Ω	67	43-44	0
4-47	LG	1, 50, 100 Ω	33	3-4	0
9-53	LG	1, 50, 100 Ω	33	9-53	0

Source: Authors

5.10 SIMULATION RESULTS FOR THE 134-BUS DISTRIBUTION SYSTEM

The proposed method performance was also verified on the 134-bus system shown in Figure 23 (134-bus system data is available in [10]).

Figure 23 – 134-bus distribution system

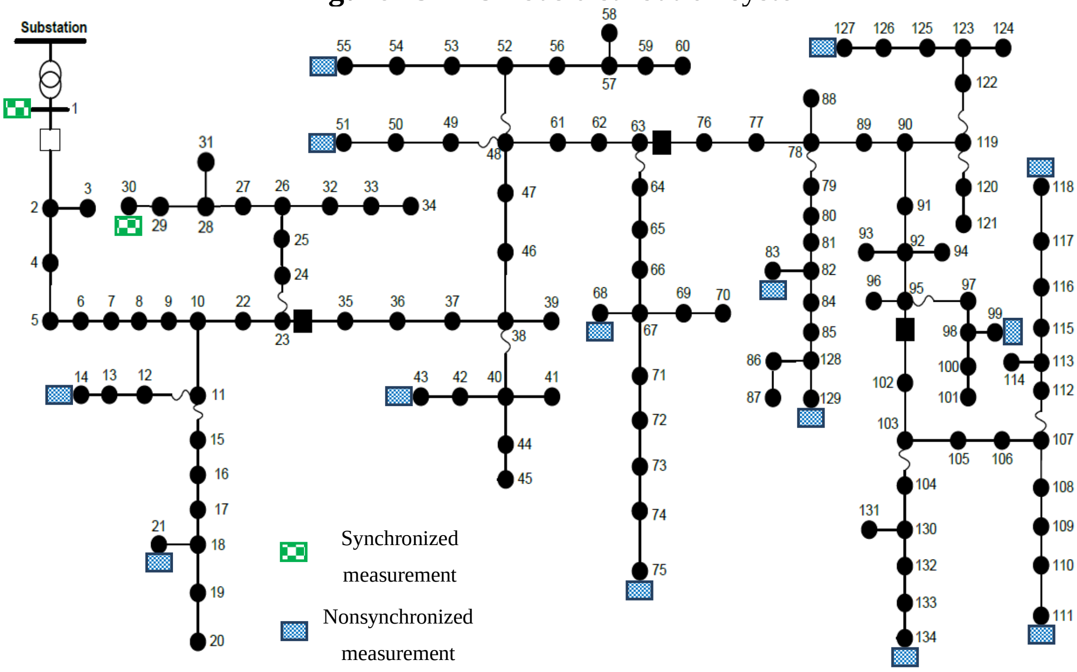

Source: Adapted from [13]

The 134-bus system has many terminal-buses with a short distance from a junction-bus, such as buses 3, 20, 31, 34, 39, 41, 45, 58, 60, 70, 87, 88, 93, 94, 96, 101, 114, and 131. Therefore, in order to reduce the number of measuring devices allocation, subsystems were not created with such terminal-buses. For example, a measuring device was not placed at bus-60, since the distance between the terminal-bus-60 and the nearest junction-bus-52 is very short (The nearest junction-bus to be considered must be present in at least one subsystem. Junction-bus-57 is not considered since it is not present in a subsystem). In this case, when a fault occurs anywhere between buses 52 and 60, bus-52 will be indicated as the fault location. Bus-52 will always be indicated as the fault location because it is present in the subsystem formed by bus-55, i.e., when a fault occurs anywhere between buses 52 and 60, bus-52 will refer to the bus closest to the fault. Since the distance between bus-52 and bus-60 is 180 meters, the maximum error for this region is 180 meters. As a criterion, measuring devices were placed at terminal-buses in which their distance to the nearest junction-bus are longer than 180 meters.

It is also important to be highlighted that there is only one section between the junction-bus-67 and the terminal-bus-68. However, the distance between such buses is 1000 meters, therefore, a measuring device was placed at bus-68.

In order to compare the proposed method performance with other methods in the literature, the simulation results obtained for the 134-bus system are described based on the distance error, calculated by (35).

$$\text{Distance Error (m)} = \left|\text{real fault distance (m) - calculated fault distance (m)}\right| \qquad (38)$$

The results of the simulation on the 134-bus system are given in Table 25 for LG fault type with/without DG presence. For all line sections, an LG fault was simulated at 50%, resulting in 133 cases. The DGs data are presented in Table 26, where their total capacity represents 28% of the total loads on the system.

As specified in Table 25, similar results are obtained for the 134-bus system when compared to the 33-bus and 69-bus systems. Although the fault location results are affected under DG presence, very good results are observed for the simulations with/without DG.

Table 25 – Simulation results for the 134-bus system

DG	**Fault type**	**Fault resistance**	**Distance Error (m)**				
			0-50	**51-100**	**101-150**	**151-200**	**201-230**
No	LG	1, 50, 100 Ω	102	24	6	1	0
Yes	LG	1, 50, 100 Ω	72	39	14	7	1

Source: Authors

Table 26 – Distributed generations installed at the 134-bus system

Bus	DG type	Capacity
3	Asynchronous (ADG)	500 kVA
98	Asynchronous (ADG)	150 kVA
51	Synchronous (SDG)	200 kVA
134	Synchronous (SDG)	100 kVA
58	Photovoltaic (PV)	500 kW
92	Photovoltaic (PV)	250 kW
123	Photovoltaic (PV)	300 kW

Source: Authors

The detailed results of the simulation on the 134-bus system are given in Table 27 and Table 28 without and with DG presence, respectively.

Table 27 – Detailed simulation results for the 134-bus system without DG

Faulted Section	Fault Type	Fault Resistance (Ω)	Actual fault distance at each section (%)	Calculated Faulted Section	Calculated fault distance at each section (%)	Distance Error (m)
1-2	L-G	50	50	1-2	48	18
2-3	L-G	50	50	1-2	96	61
2-4	L-G	50	50	2-4	0	50
4-5	L-G	50	50	2-4	92	28
5-6	L-G	50	50	5-6	36	28
6-7	L-G	50	50	6-7	36	28
7-8	L-G	50	50	7-8	36	28
8-9	L-G	50	50	7-8	88	29
9-10	L-G	50	50	7-8	92	51
10-11	L-G	50	50	10-11	0	50
11-12	L-G	50	50	11-12	48	20
12-13	L-G	50	50	12-13	84	10.2
13-14	L-G	50	50	13-14	56	9.6
11-15	L-G	50	50	11-15	12	11.4
15-16	L-G	50	50	11-15	80	11
16-17	L-G	50	50	15-16	92	10.8
17-18	L-G	50	50	17-18	24	10.4
18-19	L-G	50	50	17-18	76	29.6
19-20	L-G	50	50	17-18	76	74.6
18-21	L-G	50	50	18-21	44	9
10-22	L-G	50	50	9-10	16	57
22-23	L-G	50	50	10-22	32	55.4
23-24	L-G	50	50	22-23	20	81
24-25	L-G	50	50	23-24	88	16
25-26	L-G	50	50	24-25	96	15.8
26-27	L-G	50	50	26-27	48	20
27-28	L-G	50	50	27-28	64	5.6
28-29	L-G	50	50	28-29	52	20
29-30	L-G	50	50	29-30	72	26.4
28-31	L-G	50	50	28-29	0	10
26-32	L-G	50	50	25-26	48	25.6
32-33	L-G	50	50	25-26	48	38.1
33-34	L-G	50	50	25-26	48	53.1
23-35	L-G	50	50	22-23	24	58.2
35-36	L-G	50	50	22-23	84	56.2

36-37	L-G	50	50	35-36	24	58.2
37-38	L-G	50	50	35-36	40	57
38-39	L-G	50	50	35-36	48	86.4
38-40	L-G	50	50	35-36	48	101.4
40-41	L-G	50	50	38-40	80	50
40-42	L-G	50	50	40-42	24	13
42-43	L-G	50	50	40-42	84	12
40-44	L-G	50	50	38-40	80	35
44-45	L-G	50	50	38-40	80	70
38-46	L-G	50	50	35-36	88	58.4
46-47	L-G	50	50	46-47	44	60
47-48	L-G	50	50	47-48	44	60
48-49	L-G	50	50	47-48	96	65
49-50	L-G	50	50	49-50	48	20
50-51	L-G	50	50	50-51	52	3.4
48-52	L-G	50	50	48-52	48	20
52-53	L-G	50	50	52-53	44	3.6
53-54	L-G	50	50	53-54	52	20
54-55	L-G	50	50	54-55	88	42.9
52-56	L-G	50	50	48-52	100	10
56-57	L-G	50	50	48-52	100	60
57-58	L-G	50	50	48-52	100	125
57-59	L-G	50	50	48-52	100	130
59-60	L-G	50	50	48-52	100	170
48-61	L-G	50	50	48-61	0	20
61-62	L-G	50	50	48-61	44	27.4
62-63	L-G	50	50	48-61	96	36.6
63-64	L-G	50	50	62-63	36	47
64-65	L-G	50	50	63-64	60	22
65-66	L-G	50	50	64-65	72	20.6
66-67	L-G	50	50	65-66	68	19.6
67-68	L-G	50	50	67-68	52	20
67-69	L-G	50	50	66-67	4	29.2
69-70	L-G	50	50	66-67	4	49.2
67-71	L-G	50	50	67-71	0	25
71-72	L-G	50	50	71-72	8	16.8
72-73	L-G	50	50	72-73	12	15.2
73-74	L-G	50	50	72-73	88	14.8
74-75	L-G	50	50	74-75	40	11
63-76	L-G	50	50	62-63	48	36
76-77	L-G	50	50	63-76	16	31.8
77-78	L-G	50	50	76-77	80	31
78-79	L-G	50	50	78-79	0	35
79-80	L-G	50	50	79-80	16	23.8
80-81	L-G	50	50	79-80	92	20.6
81-82	L-G	50	50	80-81	80	21
82-83	L-G	50	50	82-83	52	20
82-84	L-G	50	50	82-84	0	25
84-85	L-G	50	50	82-84	92	19
85-128	L-G	50	50	84-85	72	18.4
128-129	L-G	50	50	128-129	52	20
128-86	L-G	50	50	85-128	12	32.6
86-87	L-G	50	50	85-128	12	57.6
78-88	L-G	50	50	77-78	48	101
78-89	L-G	50	50	77-78	92	29
89-90	L-G	50	50	78-89	88	31
90-91	L-G	50	50	90-91	36	25.2
91-92	L-G	50	50	90-91	92	24.4

92-93	L-G	50	50	90-91	96	42.2
92-94	L-G	50	50	90-91	96	62.2
92-95	L-G	50	50	92-95	28	22
95-96	L-G	50	50	92-95	76	44
95-97	L-G	50	50	95-97	20	15
97-98	L-G	50	50	97-98	32	10.8
98-99	L-G	50	50	98-99	52	20
98-100	L-G	50	50	97-98	84	29.6
100-101	L-G	50	50	97-98	84	104.6
95-102	L-G	50	50	95-102	12	22.8
102-103	L-G	50	50	102-103	0	20
103-105	L-G	50	50	103-105	40	15
105-106	L-G	50	50	105-106	48	4.2
106-107	L-G	50	50	106-107	36	4.2
107-108	L-G	50	50	107-108	48	2
108-109	L-G	50	50	108-109	52	2
109-110	L-G	50	50	109-110	72	6.6
110-111	L-G	50	50	110-111	92	8.4
107-112	L-G	50	50	107-112	48	3.4
112-113	L-G	50	50	112-113	52	2.2
113-114	L-G	50	50	113-114	0	55
113-115	L-G	50	50	113-115	56	12
115-116	L-G	50	50	115-116	60	20
116-117	L-G	50	50	116-117	64	28
117-118	L-G	50	50	117-118	72	44
103-104	L-G	50	50	102-103	48	35.8
104-130	L-G	50	50	104-130	28	15.14
130-131	L-G	50	50	104-130	80	24
130-132	L-G	50	50	130-132	52	20
132-133	L-G	50	50	133-134	12	24.8
133-134	L-G	50	50	133-134	100	20
90-119	L-G	50	50	89-90	36	87
119-120	L-G	50	50	90-119	84	52.6
120-121	L-G	50	50	90-119	84	122.6
119-122	L-G	50	50	119-122	28	15.4
122-123	L-G	50	50	122-123	52	20
123-124	L-G	50	50	125-126	52	50.8
123-125	L-G	50	50	125-126	80	42
125-126	L-G	50	50	126-127	56	42.4
126-127	L-G	50	50	126-127	100	20

Source: Authors

Table 28 – Detailed simulation results for the 134-bus system with DG

Faulted Section	**Fault Type**	**Fault Resistance (Ω)**	**Actual fault distance at each section (%)**	**Calculated Faulted Section**	**Calculated fault distance at each section (%)**	**Distance Error (m)**
1-2	L-G	50	50	1-2	44	54
2-3	L-G	50	50	1-2	96	61
2-4	L-G	50	50	2-4	0	50
4-5	L-G	50	50	2-4	72	48
5-6	L-G	50	50	5-6	5	100
6-7	L-G	50	50	5-6	72	156
7-8	L-G	50	50	7-8	32	36
8-9	L-G	50	50	7-8	88	29
9-10	L-G	50	50	7-8	32	171
10-11	L-G	50	50	9-10	0	100

11-12	L-G	50	50	11-12	52	20
12-13	L-G	50	50	13-14	24	53.4
13-14	L-G	50	50	13-14	84	54.4
11-15	L-G	50	50	11-15	32	5.4
15-16	L-G	50	50	15-16	4	4.6
16-17	L-G	50	50	16-17	32	3.6
17-18	L-G	50	50	17-18	48	0.8
18-19	L-G	50	50	18-19	0	20
19-20	L-G	50	50	18-19	0	45
18-21	L-G	50	50	18-21	52	3
10-22	L-G	50	50	10-22	0	15
22-23	L-G	50	50	22-23	0	35
23-24	L-G	50	50	23-24	0	25
24-25	L-G	50	50	23-24	96	12
25-26	L-G	50	50	25-26	16	10.2
26-27	L-G	50	50	26-27	52	20
27-28	L-G	50	50	28-29	4	60
28-29	L-G	50	50	28-29	60	100
29-30	L-G	50	50	29-30	100	60
28-31	L-G	50	50	28-29	4	50
26-32	L-G	50	50	25-26	68	19.6
32-33	L-G	50	50	25-26	68	32.1
33-34	L-G	50	50	25-26	68	47.1
23-35	L-G	50	50	8-9	0	165
35-36	L-G	50	50	10-22	12	141
36-37	L-G	50	50	22-23	20	141
37-38	L-G	50	50	22-23	36	139.8
38-39	L-G	50	50	22-23	36	174.8
38-40	L-G	50	50	22-23	36	189.8
40-41	L-G	50	50	38-40	88	42
40-42	L-G	50	50	40-42	36	7
42-43	L-G	50	50	42-43	4	4.6
40-44	L-G	50	50	38-40	88	27
44-45	L-G	50	50	38-40	88	62
38-46	L-G	50	50	22-23	84	141
46-47	L-G	50	50	46-47	36	140
47-48	L-G	50	50	47-48	44	60
48-49	L-G	50	50	47-48	96	65
49-50	L-G	50	50	49-50	48	20
50-51	L-G	50	50	50-51	80	51
48-52	L-G	50	50	48-52	56	40
52-53	L-G	50	50	53-54	4	70
53-54	L-G	50	50	53-54	64	140
54-55	L-G	50	50	54-55	100	65
52-56	L-G	50	50	52-53	100	70
56-57	L-G	50	50	52-53	100	120
57-58	L-G	50	50	52-53	100	185
57-59	L-G	50	50	52-53	100	190
59-60	L-G	50	50	52-53	100	230
48-61	L-G	50	50	48-61	0	20
61-62	L-G	50	50	48-61	64	24.4
62-63	L-G	50	50	61-62	0	35
63-64	L-G	50	50	63-64	36	4.2
64-65	L-G	50	50	64-65	40	2
65-66	L-G	50	50	65-66	48	0.6
66-67	L-G	50	50	66-67	64	2.8
67-68	L-G	50	50	67-68	56	60
67-69	L-G	50	50	67-71	12	16

69-70	L-G	50	50	67-71	12	36
67-71	L-G	50	50	67-71	68	9
71-72	L-G	50	50	71-72	84	13.6
72-73	L-G	50	50	72-73	96	18.4
73-74	L-G	50	50	74-75	12	23.2
74-75	L-G	50	50	74-75	76	6.6
63-76	L-G	50	50	62-63	96	12
76-77	L-G	50	50	76-77	0	15
77-78	L-G	50	50	77-78	40	5
78-79	L-G	50	50	78-79	52	1.4
79-80	L-G	50	50	79-80	64	9.8
80-81	L-G	50	50	81-82	8	17.4
81-82	L-G	50	50	82-84	12	21
82-83	L-G	50	50	82-83	56	60
82-84	L-G	50	50	84-85	4	26.2
84-85	L-G	50	50	85-86	80	31
85-128	L-G	50	50	85-128	100	10
128-129	L-G	50	50	128-129	60	100
128-86	L-G	50	50	128-129	4	55
86-87	L-G	50	50	128-129	4	80
78-88	L-G	50	50	77-78	96	67
78-89	L-G	50	50	77-78	32	59
89-90	L-G	50	50	89-90	16	17
90-91	L-G	50	50	90-119	4	94.4
91-92	L-G	50	50	91-92	92	8.4
92-93	L-G	50	50	92-95	8	23
92-94	L-G	50	50	92-95	8	45
92-95	L-G	50	50	92-95	64	14
95-96	L-G	50	50	95-97	48	44
95-97	L-G	50	50	97-98	4	27.4
97-98	L-G	50	50	97-98	100	30
98-99	L-G	50	50	98-99	60	100
98-100	L-G	50	50	98-99	4	60
100-101	L-G	50	50	98-99	4	135
95-102	L-G	50	50	95-102	92	25.2
102-103	L-G	50	50	103-105	8	32
103-105	L-G	50	50	103-105	76	39
105-106	L-G	50	50	105-106	80	63
106-107	L-G	50	50	107-108	64	79
107-108	L-G	50	50	108-109	28	78
108-109	L-G	50	50	109-110	92	77.6
109-110	L-G	50	50	110-111	100	35
110-111	L-G	50	50	110-111	100	10
107-112	L-G	50	50	112-113	16	102.6
112-113	L-G	50	50	113-115	20	95
113-114	L-G	50	50	113-115	44	143
113-115	L-G	50	50	113-115	100	100
115-116	L-G	50	50	116-117	12	124
116-117	L-G	50	50	117-118	24	148
117-118	L-G	50	50	117-118	100	100
103-104	L-G	50	50	103-104	40	3.48
104-130	L-G	50	50	104-130	52	1.4
130-131	L-G	50	50	130-131	0	10
130-132	L-G	50	50	130-132	56	60
132-133	L-G	50	50	133-134	100	60
133-134	L-G	50	50	133-134	100	20
90-119	L-G	50	50	90-119	60	11
119-120	L-G	50	50	119-122	28	54.6

120-121	L-G	50	50	119-122	28	124.6
119-122	L-G	50	50	119-122	84	23.8
122-123	L-G	50	50	122-123	60	100
123-124	L-G	50	50	126-127	100	110
123-125	L-G	50	50	126-127	100	90
125-126	L-G	50	50	126-127	100	60
126-127	L-G	50	50	126-127	100	20

Source: Authors

6. DISCUSSIONS AND COMPARISONS

In this work, the proposed method is evaluated on three different distributions systems (33, 69, and 134-bus systems). Since such distribution systems are also used in other methods, comparisons can be made in order to further investigate the method performance.

6.1 DISCUSSIONS AND COMPARISONS WITH REFERENCE [16]

In [16], a method for fault location is proposed for distribution systems. For such a method, loads data must be known, as well as nonsynchronized voltage measurements at the substation-bus and at all terminal-buses. The accuracy of the method proposed in [16] is evaluated on the 69-bus system, where faults were simulated at 33% and 67% of all line sections. Such a method does not work for LLL faults and only inverter-interfaced DGs are addressed. Since several simulation results are presented, the best simulation results provided in [16] are adopted for comparative purposes. The best simulation results of the method proposed in [16], without DG, indicate 123 correct sections and 11 adjacent sections.

The performance of the method proposed in this work is described in Table 23 for the 69-bus system. From 136 cases, 120 correct sections and 16 adjacent sections are indicated for LG fault in a scenario with DG. As can be noted, even considering DG, the method introduced in this work presented results very similar to the best simulation results in [16]. Furthermore, our method indicates the “correct half” and, in some cases, the “exact point” of the faulted section correctly, which is not provided in [16].

6.2 DISCUSSIONS AND COMPARISONS WITH REFERENCES [10], [17], [18], AND [21]

The methods proposed in [10], [17], [18], and [21] are also validated on the 134-bus systems, where the errors were also calculated by (35).

The performance of the method introduced in this work, on the 134-bus system, is specified in Table 25. When compared to other methods results, very good results are obtained even under DG presence. With and without DG, the method proposed in this work provides a distance error from 0 to 50 meters in most of the cases. Only in a case, a fault is indicated in the wrong place with a distance error of 230 meters. Such results are obtained by using 16 measuring devices.

In [21], a method for fault location in distribution networks is proposed. Synchronized and nonsynchronized measurements are required at a few buses. Furthermore, the voltage sag at buses with DG must be measured synchronously. In a scenario with 3 DGs, 18 measuring devices were considered during the simulations performed in [21]. In most cases, the distance error also ranges from 0 to 50 meters and, in some cases, an error distance of 220 meters is obtained. Therefore, similar results can be verified when the method proposed in this work is compared to the method proposed in [21]. On the other hand, the method proposed in [21] locates the faulted bus. Hence, when a fault occurs along a line section the method accuracy is reduced since the bus closest to the fault is pinpointed.

The methods proposed in [10], [17], and [18] provided distance errors from 0 to 100 meters in most of the cases, and errors higher than 400 meters in some cases. Therefore, from such comparisons, for LG fault, the very good performance of our method can be verified under DG presence. It must also be highlighted that DGs are not addressed in [10], [17], [18].

7. CONCLUSIONS

This work introduces a new method for fault location in distribution networks based on classical circuit analyses. As input data, the method requires only line sections impedance along with voltage measurements at the substation-bus and terminal-buses, and loads data are not required. The number of terminal-buses to be equipped with measuring can vary according to the desired distance accuracy.

Due to the subsystems concept proposed in this work, the fault location process is performed by solving determined systems of equations, which makes the method more technically accessible than the existing methods.

During the fault location process, some impedance-based methods, such as [22], locate the fault at totally different laterals with the same fault impedance between the substation and the fault location. Hence, significant distance errors are obtained. In this work, the procedure of investigating the subsystems/laterals separately prevents the fault of being located at different laterals.

The methods in the literature, addressing DG penetration, require synchronized measurements at buses with DG. In order to reduce the number of measuring devices, in this work, a new concept is presented during the fault current calculation, where measurements are not required at buses with DG.

During the validation of the proposed method, different scenarios were tested to verify the sensitivity of the method with and without DG presence. The method behaved very well for all fault types under a large range of fault resistance, line parameter errors, voltage measurement errors, and high loading and unbalanced system conditions. Although the method performance is affected under DG presence, very good results are achieved when compared with other methods proposed in the literature, mainly for LG fault.

As discussed, methods that consider DG require synchronized measurements for each DG unit. Therefore, as a proposal for future work, it would be interesting to investigate the behavior of the proposed method when non-synchronized measurements are adopted at buses with DG. Although attractive results are already obtained, such analyses could further improve the performance of the method in the presence of DG.

Preliminary analyses were carried out by inserting additional synchronized meters in the network. With additional measuring devices, some subsystems could be partitioned, i.e., one subsystem was transformed into two. Although additional meters have been inserted, the number of additional meters is lower than the number of DGs, which is also more attractive than the procedures proposed in the literature. As a result, such a procedure increased the accuracy of the proposed method as the effects of some DGs are eliminated (DGs located outside the new subsystems). However, more investigations must be made.

REFERENCES

[1] KEZUNOVIC, M. Smart fault location for smart grids," *IEEE Transaction. Smart Grid*, Piscataway, v. 2, n. 1, p. 11–22, 2011.

[2] GURURAJAPATHY, S. S. ; MOKHLIS, H.; ILLIAS, H. A. Fault location and detection techniques in power distribution systems with distributed generation: A review. *Renewable Sustain. Energy Review*, v. 74, p. 949–958, 2017.

[3] SHAFIULLAH, M. ; ABIDO, M. A review on distribution grid fault location techniques. *Journal of Electric Power Components and Systems*, v. 45, n. 8, p. 807-824, 2017.

[4] FARAJOLLAHI, M.; FOTUHI-FIRUZABAD, M.; SAFDARIAN, A. Deployment of fault indicator in distribution networks: a MIP-based approach. *IEEE Transaction. Smart Grid*, Piscataway, v. 9, n. 3, p. 2259–2267, 2018.

[5] LEE, L. A. ; CENTENO, V. Comparison of µPMU and PMU. *in*: CLEMSON UNIVERSITY POWER SYSTEMS CONFERENCE (PSC), 2018, Charleston. *Proceedingns* [of the…]. Charleston: IEEE, 2018.

[6] PEREIRA, R. A. F.; SILVA L. G. W. ; KEZUNOVIC, M. ; MANTOVANI, J. ; MANTOVANI, R. S. Improved fault location on distribution feeders based on matching during fault voltage sags. *IEEE Transaction Power Delivery,* Piscataway, v. 24, n. 2, p. 852–862, 2009.

[7] LIAO, Y. Generalized fault location methods for overhead electric distribution systems. *IEEE Transaction Power Delivery,* Piscataway, v. 26, n. 1, p. 53–64, 2011.

[8] KRISHNATHEVAR, R. ; NGU, E. E. Generalized impedance-based fault location for distribution systems. *IEEE Transaction Power Delivery,* Piscataway, v. 27, n. 1, p. 449–451, 2012.

[9] LOTFIFARD, S.; KEZUNOVIC, M.; MOUSAVI, M. J. Voltage sag data utilization for distribution fault location. *IEEE Transaction Power Delivery*, Piscataway, v. 26, n. 2, p. 1239–1246, 2011.

[10] TRINDADE, F. C. L.; FREITAS, W.; VIEIRA, J. C. M. Fault location in distribution systems based on smart feeder meters. *IEEE Transaction Power Delivery,* Piscataway, v. 29, n. 1, p. 251–260, 2014.

[11] DONG, Y.; ZHENG, C.; KEZUNOVIC, M. Enhancing accuracy while reducing computation complexity for voltage-sag-based distribution fault location. *IEEE Transaction Power Delivery,* Piscataway, v. 29, n. 1, p. 251–260, 2014.

[12] REN, J.; VENKATA, S. S.; SORTOMME, E. An accurate synchrophasor based fault location method for emerging distribution systems. *IEEE Transactions Power Delivery*, Piscataway, v. 29, n. 1, p. 297–298, 2014.

[13] BÍSCARO, A. A. P.; PEREIRA, R. A. F.; KEZUNOVIC, M.; MANTOVANI, J. R. S. Integrated fault location and power-quality analysis in electric power distribution systems. *IEEE Transactions Power Delivery*, Piscataway, v. 31, n. 2, p. 428– 436, 2016.

[14] MANASSERO, G.; DI SANTO, S. G.; SOUTO, L. Heuristic method for fault location in distribution feeders with the presence of distributed generation. *IEEE Transactions Smart Grid*, Piscataway, v. 8, n. 6, p. 2849–2858, 2017.

[15] JIA, K. ; BI, T.; REN, Z.; THOMAS, D.; SUMNER, M. High frequency impedance-based fault location in distribution system with DGs. *IEEE Transactions Smart Grid*, Piscataway, v. 9, n. 2, p. 807–816, 2018.

[16] JIA, K. ; YANG, B.; DONG, X.; FENG, T.; BI, T.; THOMAS, D. Sparse voltage measurement-based fault location using intelligent electronic devices. *IEEE Transactions Smart Grid*, Piscataway, v. 11, n. 1, 2020.

[17] MAJIDI, M.; ETEZADI-AMOLI, M.; FADALI, M. S. A novel method for single and simultaneous fault location in distribution networks," *IEEE Transactions Power Systems*, Piscataway, v. 30, n. 6, p. 3368–3376, 2015.

[18] MAJIDI, M.; ARABALI, A.; ETEZADI-AMOLI, M. Fault location in distribution networks by compressive sensing. *IEEE Transactions Power Delivery*, Piscataway, v. 30, n. 4, p. 1761–1769, 2015.

[19] CARTA, D. ; PEGORARO, P. A. ; SULIS, S. Impact of measurement accuracy on fault detection obtained with compressive sensing. *In:* INTERNATIONAL WORKSHOP ON APPLIED MEASUREMENTS FOR POWER SYSTEMS (AMPS), 9, 2018, Bologna. *Proceedings* [of the]. Bologna: IEEE, 2018. p. 1–5.

[20] TRINDADE, F. C. L. ; FREITAS, W. Low voltage zones to support fault location in distribution systems with smart meters. *IEEE Transactions on Smart Grid*, Pisacataway, v. 8, n. 6, p. 2765-2774, 2017.

[21] MAJIDI, M.; ETEZADI-AMOLI, M. A new fault location technique in smart distribution networks using synchronized/nonsynchronized measurements. *IEEE Transactions Power Delivery*, Piscataway, v. 33, n. 3, p. 1358–1368, 2018.

[22] BRAHMA, S. M. Fault location in power distribution system with penetration of distributed generation. *IEEE Transactions Power Delivery*, Pisacataway, v. 26, n. 3, p. 1545–1553, 2011.

[23] ALWASH, S. F. ; RAMACHANDARAMURTHY, V. K.; MITHULANANTHAN, N. Fault location scheme for power distribution system with distributed generation," *IEEE Trans. Power Del.*, vol. 30, no. 3, pp. 1187–1195, Jun. 2015.

[24] M. Pignati and L. Zanni *et al.*, "Fault detection and faulted line identification in active distribution networks using synchrophasors-based real-time state estimation. *IEEE Transactions Power Delivery*, Piscataway, v. 32, n. 1, p. 381–392, 2017.

[25] SUN, K.; CHEN, Q.; GAO, Z. An automatic faulted line section location method for electric power distribution systems based on multisource information. *IEEE Transactions Power Delivery*, Piscataway, v. 31, n. 4, p. 1542-1551, 2016.

[26] TENG, J. ;HUANG, W. ;LUAN, S. Automatic and fast faulted line-section location method for distribution systems based on fault indicators. *IEEE Transactions Power Systems*, Pisacataway, v. 29, n. 4, p. 1653-1662, 2014.

[27] KIAEI, I.; LOTFIFARD, S. Fault section identification in smart distribution systems using multi-source data based on fuzzy petri nets. *IEEE Transactions Smart Grid*, Piscataway, v. 11, n. 1, 2019.

[28] DIgSILENT, [Online]. Available: http://www.digsilent.de/

[29] REN, F. ; ZHANG, M.; SUTANTO, D. A multi-agent solution to distribution system management by considering distributed generators. *IEEE Transactions Power Systems*, Piscataway, v. 28, n. 2, p. 1442–1451, 2013.

[30] YAZDANPANAHi, H. ; LI, Y. W. ; XU, W. A new control strategy to mitigate the impact of inverter-based DGs on protection system. *IEEE Transactions Smart Grid*, v. 3, n. 3, p. 1427–1436, 2012.

[31] BARAN, M. E. ; WU, F. F. Network reconfiguration in distribution systems for loss reduction and load balancing. *IEEE Transactions on Power Delivery*, Piscataway, v. 4, p. 1401-1407, 1989.

[32] BARAN, M. E. ;WU, F. F. Optimal capacitor placement on radial distribution feeders. *IEEE Transactions on Power Delivery*, Piscataway, v. 4, n. 1, p. 725-734, 1989.